Dynamics and Stability Analysis of a Lander Considering Large Amplitude Propellant Sloshing

Master Thesis

Dynamics and Stability Analysis of a Lander Considering Large Amplitude Propellant Sloshing

(大振幅燃料スロッシングを考慮した着陸機のダイナミクスおよび安定性解析)

August 2019

Supervisor: Prof. Tatsuaki Hashimoto

Department of Electrical Engineering and Information Systems,

School of Engineering, The University of Tokyo

37-175086　Mohammad Khaled Alqudah

Abstract

Landing missions are of high importance in space exploration. A successful touchdown on a celestial body surface is essential for sample return missions and deployment of exploration technology such as rovers. Consequently, over the years a lot of research has been dedicated for landing operations, such research includes landing trajectory optimization, landing gear design, footpad design, and so on. In these studies spacecrafts and landers are often considered as rigid bodies with landing gears and in few cases flexible components, but the presence of large disturbances such as propellant sloshing is not taken into consideration.

So far, little or no research has been conducted to examine the effects of large amplitude sloshing on a lander's dynamics during touchdown and landing. Therefore, the purpose of this research is to investigate the effects of large amplitude propellant sloshing on planetary landers and small celestial body landers under varying landing conditions. To do so, a lander simulation model is developed using MATLAB software. The lander is modelled as a rigid body with landing gear and propellant slosh dynamics. Propellant sloshing is modelled using a mass-spring-damper equivalent mechanical model. To provide a thorough and comprehensive analysis, celestial bodies with both high and low gravity fields are considered in the simulations. Several landing scenarios are simulated with varying conditions and the behavior of the lander is analyzed with and without propellant sloshing. The effect of propellant sloshing on the spacecraft attitude and translation motion is studied for all the cases.

Acknowledgement

I wish to express my sincere gratitude to my supervisor, Professor Tatsuaki Hashimoto, for his guidance and supervision throughout the course of this research study. I would also like to pay special thanks to Dr. Takao Maeda for his valued help and support at the early stages of this study. In addition, I am grateful for the wonderful opportunity and constant support provided by the Department of Electrical Engineering and Information Systems and the IME department at the University of Tokyo. I also wish to acknowledge my friends and colleagues, Abdulla Ayyad in particular, for their joyful company during the long days of work and study.

Table of Contents

List of Figures

List of Tables

1. Introduction

1.1. Motivation

Spacecrafts usually have complicated structures with rigid platforms, flexible components such as different kinds of appendages and solar arrays, and more often than not fluid propellants. The existence of these different components and the coupling effects that arise between these systems is a main cause of the difficulty and sensitivity of space missions. One phenomenon that can impose significant disturbances on a spacecrafts' dynamics is sloshing of liquid propellants inside the tank walls. During sample return and lander missions, the spacecraft utilizes significant amount of fuel. When the spacecraft reaches the target body, the fuel tanks are about half full and this is when sloshing effects are most severe. At touchdown the spacecraft is subjected to substantial forces and torques that can result in high amplitude propellant sloshing. Numerous research studies have been conducted with the purpose of studying the effects of propellant sloshing on spacecraft attitude and position. However, most of these studies address propellant sloshing under low excitation for the purposes of attitude control, pointing accuracy, and stabilization. So far, little or no research has been conducted to examine the effects of large amplitude sloshing on a spacecrafts' dynamics during touchdown and landing. Therefore, the aim of this research is to model the dynamics of a lander with large amplitude sloshing and study the effects of propellant sloshing on the behavior of the system. To provide a thorough and comprehensive study we consider both planetary landers and small celestial body landers such as asteroid landers.

1.2. Spacecraft Case Studies and Failures

There are several examples of space missions where the spacecraft showed abnormal behavior resulting in mission delays, minor failures, or even complete mission failure with one

possible cause being propellant sloshing in the spacecraft tanks. Some examples of such cases include:

1. INTELSAT IV series spacecraft (1974): During an extensive series of in-orbit tests, the spacecraft, which carried liquid hydrazine in four propellant tanks, experienced unstable attitude nutation effects [1].

2. ATS-V Satellite (1969): After upper stage burnout, the spacecraft, which weighed around 450 kg carrying only 1.2 kg of liquid propellant, experienced uncontrollable divergent nutation behavior, causing the spacecraft to enter a flat spin and resulting in mission loss. This shows that even small amount of liquid propellant can cause catastrophes [2].

4. NEAR shoemaker (1998): During the rendezvous mission to asteroid Eros, the spacecraft experienced an abnormal series of attitude motions during its reorientation maneuver and went into safety mode causing a 13-month delay in the mission. Propellant sloshing was identified as the probable cause [3].

5. Apollo 11 Lunar Module (1969): During the last moments of the lunar landing, the spacecraft experienced problems with the landing maneuver control due to sloshing of the remaining propellant [4].

6. LEASAT mission (1984): Instabilities in the control systems of both the first and second LEASAT spacecrafts were observed during the missions. Propellant sloshing frequency was identified as the most likely cause of the instabilities [5].

7. Chang'e 3 lunar probe (2013): While carrying out the soft landing mission on the lunar surface, liquid propellant sloshing caused the spacecraft to experience instability in its motion. Although the lander kept a vertical attitude, it underwent a rocking back and forth motion horizontally [6].

8. Solar Dynamics Observatory (2010): Launched and deployed from Atlas V launch vehicle, the spacecraft had two large propellant tanks. Abnormal attitude behavior was observed during the second apogee motor firing and the cause was linked to propellant sloshing [7].

9. DemoSat (2007): After second stage ignition, the spacecraft experienced a divergent circular coning oscillation because of propellant sloshing. As a result, the spacecraft failed to reach its target orbit [8].

1.3. Lander Descent Phase

In a lander mission, typically, the descent phase comprises of sub-phases designed to achieve the highest probability of successful landing. For instance, in the Altair lunar lander mission, the descent phase is comprised of three sub-phases: the braking phase, the approach phase, and the terminal descent and touchdown phase [9]. These subphases are demonstrated in Fig. 1.

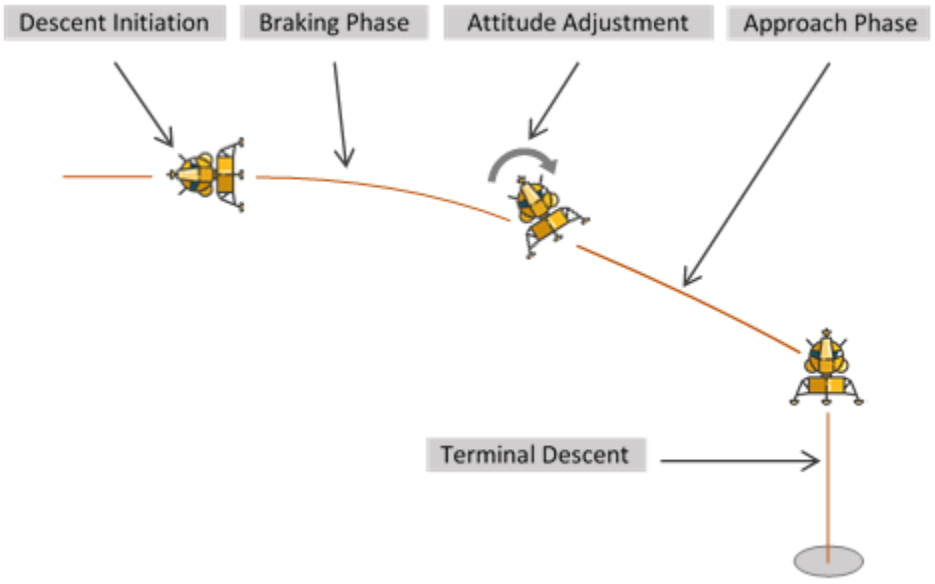

Figure 1: Sub-phases during descent and touchdown.[9]

The braking phase starts at the descent orbit altitude of about 15 km, during the braking phase the orbital speed of the vehicle is significantly and efficiently reduced. The vehicle then

performs a pitch up maneuver to adjust the attitude of the spacecraft in preparation for landing. The approach phase is then carried out bringing the vehicle near the surface at altitude of about 30 m above touchdown site. Lastly the terminal descent takes place, the thrusters are shutdown when the vehicle is close to the surface (about 1 m), which means the vehicle experiences a short period of freefall just prior to touchdown.

During this research we focus our analysis on the last portion of the terminal descent phase. We wish to evaluate the effects of propellant sloshing on the stability and behavior of a lander in a ballistic touchdown.

1.4. Literature Review

1.4.1. Propellant Sloshing

1.4.1.1. Overview

Research studies on propellant sloshing have been conducted since the beginning of the 1960s. Space vehicle require significant amounts of fuel for various space operations such as trajectory maneuvers, momentum dumping, and attitude control [10]. As a space mission goes on, fuel is being consumed and the fill level of the tank decreases, which has a significant effect on slosh, as the fill level of the decreases sloshing increases within the tank walls, sloshing is maximum when the tank is about half full. The uncontrollable motion of propellant in partially filled tanks introduces a major source of disturbance on the spacecraft dynamics which can cause several problems such attitude instability, pointing accuracy degradation, and nutation behavior. As a result, many engineers and scientists were motivated to design control systems for vehicles considering the dynamic interaction of propellant sloshing [11,12,13]. Numerous analytical and experimental work has been conducted to study the stability of spacecraft taking into consideration the effects of propellant sloshing [14,15,16]. The development of multibody

dynamics allowed to successfully predict attitude motion and behavior of space vehicles taking into consideration the effect of propellant sloshing [17,18,19].

1.4.1.2. Modelling

The exact formulation and simulation of propellant sloshing in various types of tanks is a complex problem. The most accurate method to simulate the dynamics of propellant slosh is by using computational fluid dynamics (CFDs). However, CFDs require high computational cost and therefore not a feasible solution for online simulation and control purposes [20]. As a result, dynamically equivalent mechanical models (EMMs) have been developed and adopted to model and approximate the behavior of propellant slosh. In their slosh design handbook, Roberts et al. described several equivalent mechanical models for sloshing [21]. Kana [22] proposed a compound pendulum model including spherical and planar pendulums to model propellant sloshing in a rotary tank. Mason and Starin examined the effects of propellant sloshing dynamics on the Solar Dynamics Observatory [7], a three-axis controlled, single fault tolerant spacecraft. The study determined that an anomaly that occurred during motor firing was due to sloshing dynamics. Nan et al. considered a composite equivalent model to estimate slosh forces and moments exerted on a spherical tank in a spacecraft [23]. A three-dimensional model for maneuvering of a spacecraft with unactuated propellant sloshing was presented by Navabi et al. using Lagrange method [24]. A multi pendulum model was adopted to simulate sloshing dynamics, see Fig. 2.

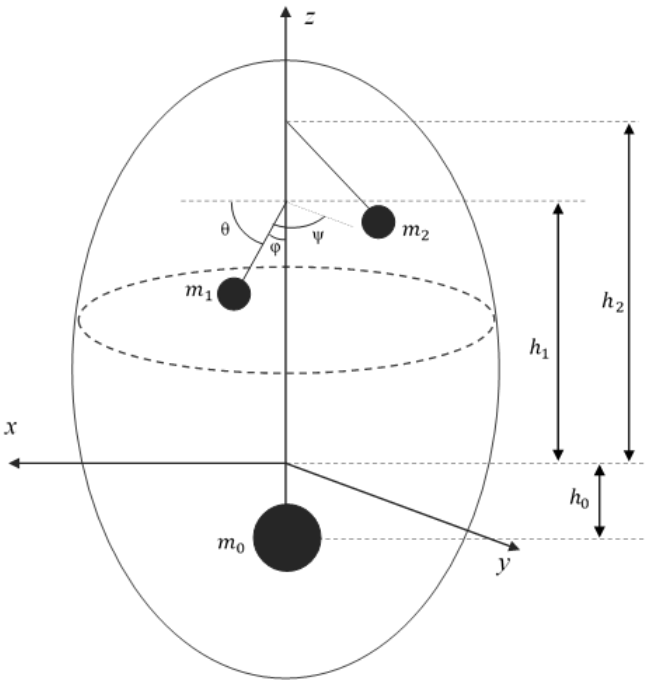

Figure 2: Three-dimensional multi pendulum model for propellant sloshing.[24]

Hervas and Reyhanoglu [25] considered a multi-mass-spring model to characterize propellant sloshing, see Fig. 3. They designed a lyapunov-based nonlinear controller for a spacecraft with propellant slosh to control attitude and velocity.

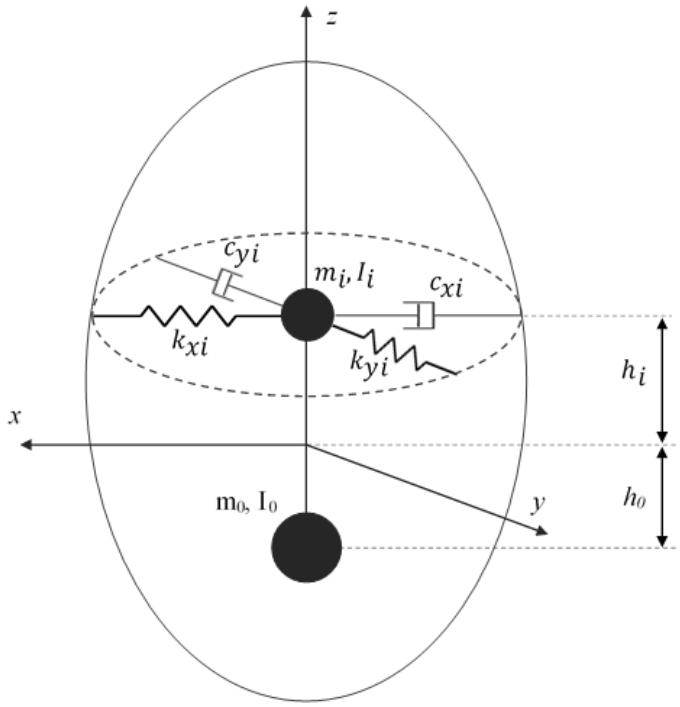

Figure 3: Multi mass-spring model of propellant sloshing.[25]

In recent years, research studies started to model spacecrafts as a combination of rigid bodies, flexible appendages and propellant slosh EMMs. Deng and Yue studied the dynamics and control of a spacecraft with large amplitude propellant slosh [26]. In their work, they used an improved moving pulsating ball model to simulate propellant slosh dynamics, see Fig. 4.

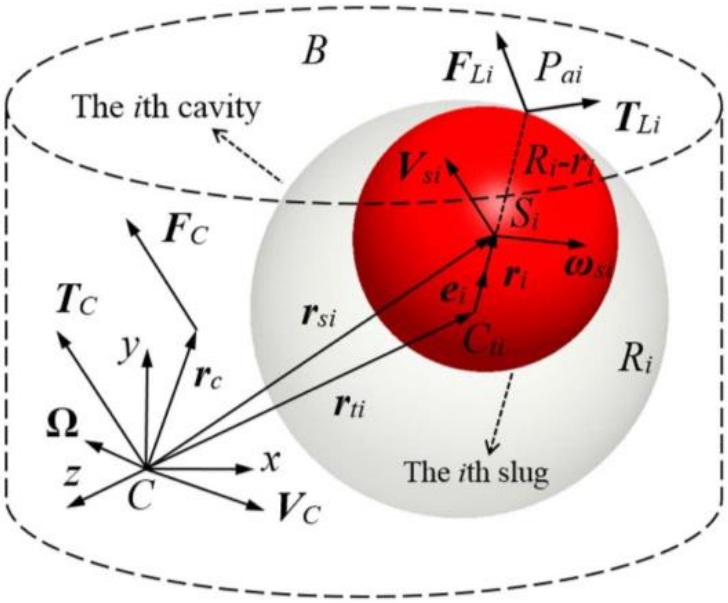

Figure 4: Moving pulsating ball model for propellant sloshing.[26]

1.4.2. Small Celestial Body Landers

1.4.2.1. Overview

In recent years, several space missions have been conducted with the purpose of exploring small celestial bodies. It is believed that small celestial bodies such as asteroids and comets have the least processed material in the solar system, this is because their size is too small to have high internal pressures and temperatures. It is most probable that even pre-solar grains still reside in these bodies. Therefore, information about their physical properties and composition are of great scientific value [27,28]. As a result, sample return missions to small celestial bodies have been gaining momentum over the past years.

1.4.2.2. Missions

On February 12 of 2001, the first successful asteroid landing was achieved by the Near Earth Asteroid Rendezvous (NEAR) Spacecraft which descended onto the surface of asteroid 433 Eros [29]. The spacecraft was planned to perform four braking maneuvers to bring the descent velocity to 1.3 m/s at impact. However, when NEAR reached the surface the target velocity had not been achieved, the estimated speed of impact was around 1.6 m/s, which caused it to continue burning pushing the vehicle into the asteroid. Eventually it came to rest and data was received from the spacecraft proving it survived the impact. A major challenge during the descent was the significant delay in communication.

In 2003 the Japan Aerospace Exploration Agency (JAXA) launched the robotic spacecraft Hayabusa to retrieve a sample material from the near Earth asteroid Itokawa [30]. The spacecraft rendezvoused with the asteroid in 2005. Hayabusa spacecraft stayed in close proximity to asteroid Itokawa for three months mapping the surface prior to descent. The spacecraft then successfully performed a touch-and-go landing retrieving a sample from the asteroids surface. Following the successful return of Hayabusa, JAXA launched the spacecraft Hayabusa 2 for another asteroid sample return mission to near Earth asteroid Ryugu [31].

In March of 2004, the European Space Agency (ESA) launched the Rosetta spacecraft targeting comet 67P/Churyumov-Gerasimenk. The main scientific objective of the Rosetta mission was to study the origins of the solar system through examining comets and their origins. The mission contained two main components; the orbiter spacecraft Rosetta, and its lander Philae. In 2014 the lander, Philae, was able to successfully land on the comets' surface after separating from Rosetta spacecraft at an altitude of about 1 km [28,32,33].

1.4.2.3. Challenges and Failures

Landing on the surfaces of small celestial bodies such as asteroids and comets is not an easy task due to several factors. The extreme low gravity conditions make it far more difficult

to stabilize the spacecraft upon touchdown. The unknown or unanticipated surface conditions can increase the chances of undesired behavior. Furthermore, sample return missions to small celestial bodies usually require deep space voyages, resulting in huge communication delays which, as a result, further increases the need for a successful fully autonomous operation.

In the case of the Rosetta spacecraft lander, Philae, a failure of the anchoring harpoons and thrusters occurred during touchdown sequence causing the lander to bounce off the surface after initial touchdown with a high rebound velocity of 0.38m/s (escape velocity was ≈ 0.44m/s). The lander started tumbling and reached an altitude of about 1 km after the first bounce before starting to descend again. Upon impacting the surface again, the lander bounced a second time before coming to rest next to a cliff about a kilometer away from the intended landing site [34,35].

During the Hayabusa mission, the spacecraft experienced failure of two attitude control reaction wheels prior to the descent operation, causing the LIDAR to have oddly large measurement errors. Due to the failures, it was not possible for the Hayabusa spacecraft to approach asteroid Itokawa autonomously as initially planned. Consequently, the guidance and navigation operation for the descent phase had to be redesigned.

1.5. Research Objectives and Thesis Overview

1.5.1. Research Contribution & Objectives

Numerous research studies have been conducted with the purpose of studying the effects of propellant sloshing on spacecraft dynamics. However, most of these studies address propellant sloshing under low excitation for the purposes of attitude control, pointing accuracy, and stabilization. So far, little or no research has been conducted to examine the effects of large amplitude sloshing on a spacecrafts' dynamics during touchdown and landing.

Therefore, the aim of this research is to investigate the effects of large amplitude propellant sloshing on a lander during touchdown and landing. The overall objective is to provide a comprehensive and thorough analysis of the behavior of a lander in the presence of large disturbances such as propellant sloshing under different conditions and varying parameters. The research focuses on the last phase, the terminal descent phase, of a landing operation. The analysis covers cases where a significant gravitational pull is present as in the case of lunar landing and cases where the gravitational field is extremely small as in the case of asteroid and comet landing.

1.5.2. Method of Approach

A lander simulation model is developed to examine the effects of propellant sloshing during touchdown and landing. The simulation model consists of four main components; the lander rigid body model, the landing gear model, the propellant slosh model, and the celestial body surface interaction model. The lander rigid body is modelled as a cubic rigid structure with landing legs. For the purposes of this research, the presence of flexible structures such as solar arrays and appendages is not considered. The four landing gears are modelled as spring damper systems connecting the landing footpads to the edges of the lander body. Propellant sloshing is characterized using spring-mass-damper models. In the case of low gravity simulations, a modified spring-mass-damper model is used to model large amplitude propellant sloshing. Lastly, to model the interaction of the landing footpads with surface of the celestial body, virtual spring-damper models are used between each footpad and the surface while also accounting for frictional forces. The systems equations of motion are derived and expressed as a differential algebraic equation and solved using a 4^{th} order Runge-Kutta solver using MATLAB software.

1.5.3. Thesis Overview

This thesis is divided into 3 main sections. Chapter 2 explains the lander dynamics with propellant sloshing in details. The propellant sloshing equivalent mechanical models are presented and slosh forces and moments are derived. The interaction model between the lander and the surface of the celestial body is presented in detail and touchdown forces and torques are derived. The equations of motion of the lander rigid body are derived taking into account landing gear forces and moments, slosh forces and moments, and the interaction between the lander and the celestial body surface.

Chapter 3 covers the landing simulations and results. First an overview of the simulation setups is presented. Simulations are divided into two main sections, the first section covers landing simulation in the case of low gravity field, and the second sections covers landing simulations in the case of high gravity field. For both cases, the effects of propellant sloshing are investigated against several factors such as surface conditions, lander velocity, lander geometry, etc.

Chapter 4 discusses attitude stabilization of landers using variable damper landing gears. This concept was introduced by Maeda et al. [36] in their paper published in 2016, where they propose improving the stability of a lunar lander using a variable damper landing gear. In chapter 4, the effectiveness of the variable damper landing gear is examined in the presence of large disturbances such as propellant sloshing for high gravity conditions.

2. Spacecraft Dynamics with Propellant Sloshing

2.1. Introduction

This chapter discusses the derivation of the dynamic equations for the multibody system. As stated before, the system model consists of four main components; the lander rigid body model, the landing gear model, the propellant slosh model, and the celestial body surface interaction model. The lander is modelled as a cubic rigid structure with four landing legs. The landing gears are modelled as spring damper systems connecting the landing footpads to the edges of the lander body. Propellant sloshing is characterized using spring-mass-damper models. The sections below discuss the modelling and mathematical derivation for each component and for the whole system in details.

2.2. Propellant Sloshing Mechanical Models

2.2.1. Slosh Modelling

By definition, sloshing refers to the motion of a free liquid surface in a partially filled container as a result of any disturbance [13]. A free liquid surface can experience different types of motion such as planar, nonplanar, rotational, irregular beating, symmetric, asymmetric, quasi-periodic and chaotic. The motion of sloshing systems depends on four main variables; gravitational forces, inertia forces, capillary forces, and viscous forces. Usually, some forces are too small in comparison with other forces and can be ignored to simplify the analysis. The relative importance of the different forces can be characterized using dimensionless numbers like Weber number, Bond number, and Froude number, which separate the dynamic behavior of a sloshing system into a gravity dominated region, a capillary dominated region and an inertia dominated region [12].

In the gravity dominated region the gravitational forces are larger in comparison with capillary forces and capillary forces can be ignored. The Bond number, which is the ratio of gravitational forces to surface tension forces, is used to check if a sloshing system is within a gravity dominated region. The bond number is defined as,

$$B_o = \frac{\Delta\rho g L^2}{\gamma} \tag{1}$$

where $\Delta\rho$ is the difference in density between the two phases (liquid and gas), g is the gravitational constant, L is the characteristic length (e.g. diameter of tank), and γ is the interfacial surface tension. The system is considered to be in a gravity dominated region if $B_o \gg 1$.

In the inertia dominated region the inertia forces are larger than the capillary forces and capillary forces can be ignored. The Weber and Froude numbers are used to check if a sloshing system is within the inertia dominated region. The Weber number is defined as the ratio of inertia forces to surface tension forces and calculated as,

$$W_e = \frac{\rho v^2 L}{\gamma} \tag{2}$$

and the Froude number is defined as the ratio of inertia forces to gravitational forces and calculated as,

$$F_r = \frac{W_e}{B_o} = \frac{v^2}{gL} \tag{3}$$

where ρ is the liquid density, v is the velocity, L is the characteristic length, and γ is the surface tension. For an inertia dominated region $W_e \gg 1$ and $F_r \gg 1$.

For the capillary dominated region, capillary forces are larger compared to gravitational and inertia forces and therefore, the latter can be ignored. In addition to the above numbers, the Reynolds number is used to characterize the significance of viscous effects calculated as,

$$R_e = \frac{Lv}{\eta} \tag{4}$$

where η is the kinematic viscosity of the liquid. The Reynolds number must be determined separately for each region. Different slosh models are defined depending on which region the sloshing system falls in. In general, sloshing systems models are divided into two categories; high gravity models and low gravity models [12, 37].

In high gravity models, the magnitude of surface tension forces is insignificant and therefore ignored. High gravity models are employed when the spacecraft experiences high accelerations as in during the main engine burns. In low gravity models, surface tension forces are dominant and therefore are critical in determining the behavior of the propellant inside the tank. In general, sloshing frequencies are smaller in low gravity models than in high gravity models. Low gravity models are characterized by a very small Bond number, $B_o \ll 1$.

Several tests can be done to determine the values of the dimensionless number discussed above, such tests include spin drop tests, air bearing tests, and energy dissipation tests [38]. However, these tests are not conducted and are not within the scope of this research.

Fluid dynamics modelling most accurately simulates the behavior propellant sloshing using partial differential equations which are solved numerically using computational fluid dynamics (CFD). However, CFD require high computational costs and therefore is not a feasible solution for onboard processing and control purposes. Instead several equivalent mechanical models are used for that purpose. In the case of a fully filled tank where the propellant has no free surface, the propellant can be replaced by a rigid body. In the case of a partially filled tank, the oscillating portions of the propellant mass with a free surface are replaced by an equivalent mechanical model and the stationary potion is modelled as a rigid body [39]. For any equivalent mechanical model to be valid it should preserve the static and dynamic properties of the liquid [12]. The static properties of the liquid are preserved if the sum of all the sloshing masses and the stationary mass is equal to the mass of the liquid, and the model center of mass is at the same height as the liquid, these conditions can be expressed mathematically as,

$$m_0 + \sum_{s=1}^{N} m_s = m_{liquid} \tag{5}$$

$$m_0 h_0 + \sum_{s=1}^{N} m_s h_s = 0 \tag{6}$$

where m_0 is the stationary mass, m_s are the sloshing masses, h_0 is the position of m_0 with respect to the model center of mass, h_s are the positions of m_s with respect to the model center of mass, m_{liquid} is the mass of the liquid, and N is the number of sloshing masses in the model. In addition to satisfying the static properties conditions, the model must also preserve the dynamic properties of the liquid by reproducing the sloshing forces and moments, and the natural frequencies of the sloshing system.

This research assumes the lander contains a half-filled spherical propellant tank(s); spherical tanks are the most widely used due to the high volume to weight ratio, and sloshing is most severe at around a 50% fill level. A mass-spring-damper is used to characterize propellant sloshing, a damper component is included to account for viscous effects. Two propellant slosh models are used in this research; a modified mass-spring-damper model is used to characterize large amplitude propellant sloshing in a small celestial body lander, and a typical mass-spring-damper model is used in case of a large body lander such as a lunar lander.

2.2.2. Low Gravity Slosh Mechanical Model

In comparison to planetary landing missions such as Mars or Lunar landing, landing on small celestial bodies can be far more difficult due to the extremely low gravity. In Mars or Lunar landing, it is easy to stabilize the spacecraft after a rebound due to the presence of significant gravitational pull. However, in the case of small bodies, the gravitational pull is significantly low, and the spacecraft is more sensitive to disturbances, therefore there is a higher chance that the spacecraft cannot be stabilized after rebound or the rebound velocity is too high causing it to “fall off”. In the case of a sample return mission the propellant occupies the majority of the spacecraft mass and, therefore, it is important to consider the effects of slosh

dynamics. Large Amplitude sloshing is often excited when the spacecraft body is subjected to high acceleration as in the case of touch down, this violent sloshing can exert large forces and moments on the spacecraft body, and negatively affect its stability. In the case of a partially filled spherical tank, under low gravity conditions capillary forces become more dominant and the propellant forms a spherical interface along the tank wall, when subjected to an external disturbance the propellant is forced into a sloshing motion [40], this phenomenon is shown in Fig 5.

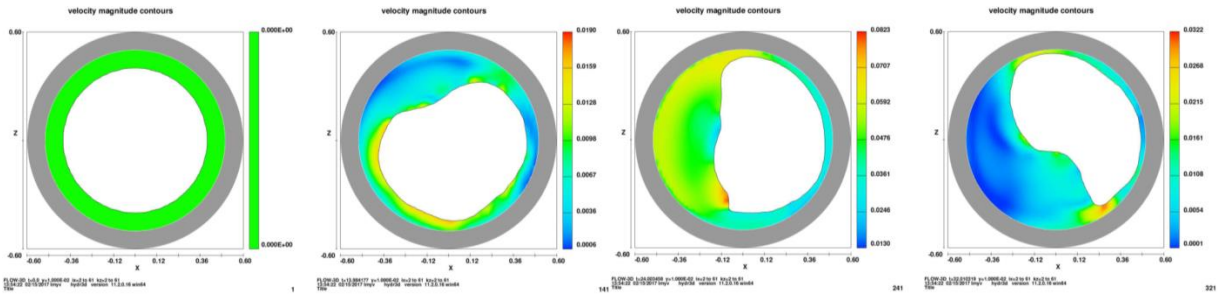

Figure 5: Result of CFD simulations for liquid behavior under low gravity.[40]

To simulate this behavior a modified mass-spring damper model is used. Although the propellant is a distributed constant system, it is modelled as concentrated constant system without considering wave motion. The propellant is modelled as a mass point constrained by a spring-damper system at the center of the tank and the mass point rotates freely about the center of the tank. Figure 6 illustrates the concept of the low gravity propellant sloshing model.

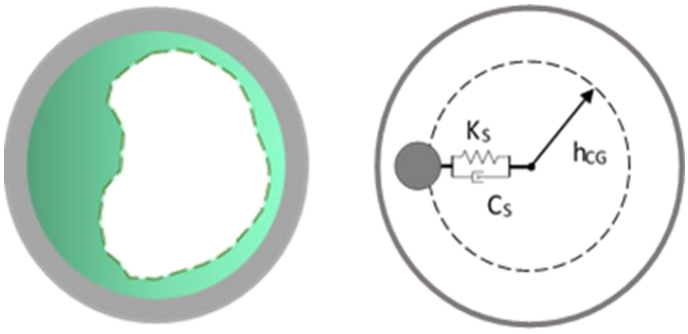

Figure 6: Low gravity propellant sloshing model.

To duplicate large amplitude sloshing at touchdown, a free motion area is introduced in the model characterized by length h_{CG}. When the spring length is less than h_{CG} spring force is not generated, so the propellant mass can move freely within a sphere of radius h_{CG} but is pulled

back by the spring when the displacement exceeds h_{CG}. The spring force always acts towards the center of the tank and the damping force acts in the opposite direction of the propellant mass velocity vector. The length h_{CG} is determined by the following equation [41],

$$h_{CG} = \frac{3a}{8}\left(\frac{1 - 2\chi^2 + \chi^4}{1 - 1.5\chi + 0.5\chi^3}\right) \tag{7}$$

where a is the radius of the tank, and the variable χ satisfies,

$$V_f = \frac{1}{4}(2 - 3\chi + \chi^3) \tag{8}$$

and V_f is the fill level of the tank. The spring and damper coefficients are determined in terms of the sloshing mass and frequency as,

$$k_s = (2\pi\omega_n)^2 \times m_s \tag{9}$$

$$c_s = 2 \times \xi \times \sqrt{k_s \times m_s} \tag{10}$$

where ω_n is the natural frequency of the sloshing system and m_s is the sloshing mass. The equation of motion of the propellant slosh is given by,

$$m_s \ddot{\boldsymbol{P}}_s = \begin{cases} -c_s \dot{\boldsymbol{P}}_s & ; \quad |\boldsymbol{P}_s| < h_{CG} \\ -k_s \boldsymbol{P}_s - c_s \dot{\boldsymbol{P}}_s & ; \quad |\boldsymbol{P}_s| \geq h_{CG} \end{cases} \tag{11}$$

where $\boldsymbol{P}_s$ is the position vector of the sloshing mass with respect to the center of the tank. The sloshing force and torque acting the body of the lander are calculated as,

$$\boldsymbol{F}_s = \begin{cases} c_s \dot{\boldsymbol{P}}_s & ; \quad |\boldsymbol{P}_s| < h_{CG} \\ k_s \boldsymbol{P}_s + c_s \dot{\boldsymbol{P}}_s & ; \quad |\boldsymbol{P}_s| \geq h_{CG} \end{cases} \tag{12}$$

$$\boldsymbol{L}_s = \boldsymbol{P}_{tank} \times \boldsymbol{F}_s \tag{13}$$

where $\boldsymbol{P}_{tank}$ is the position vector of the tank center with respect to the center of mass of the lander.

2.2.3. High Gravity Slosh Mechanical Model

In the case of landing under high gravity conditions, capillary forces are insignificant and gravitational forces dominate. The propellant accumulates on one side of the tank and sloshing occurs only at the free surface. To model propellant sloshing under high gravity, the propellant mass is divided into two parts a stationary component and an oscillating component. Because sloshing only occurs at the free surface, only planar sloshing motion is considered in the case of high gravity landing. Figure 7 illustrates the high gravity propellant sloshing model.

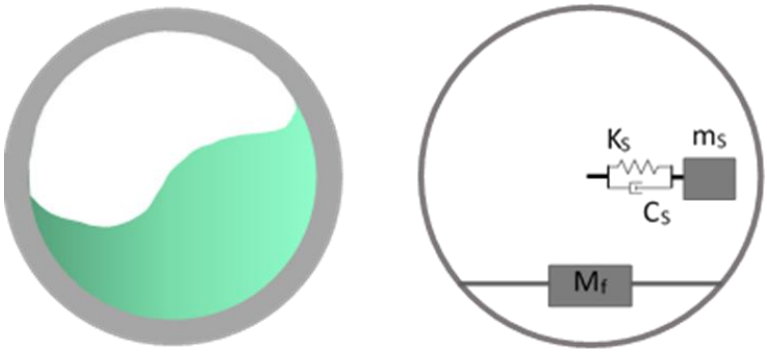

Figure 7: High gravity propellant sloshing model.

The equation of motion of the propellant sloshing system is expressed in a similar way to the case of sloshing under low gravity with the exception of not having a free motion region h_{CG}. The equation of motion for propellant sloshing under high gravity is given by,

$$m_s\ddot{\boldsymbol{P}}_s = -k_s\boldsymbol{P}_s - c_s\dot{\boldsymbol{P}}_s \tag{14}$$

where m_s is the sloshing portion of the propellant mass, and $\boldsymbol{P}_s$ is the position vector of the sloshing mas with respect to the spring damper system equilibrium point. The sloshing force and torque acting the body of the lander are calculated as,

$$\boldsymbol{F}_s = k_s\boldsymbol{P}_s + c_s\dot{\boldsymbol{P}}_s \tag{15}$$

$$\boldsymbol{L}_s = \boldsymbol{P}_{TS} \times \boldsymbol{F}_s \tag{16}$$

where $\boldsymbol{P}_{TS}$ is the position vector of the sloshing system equilibrium point with respect to the center of mass of the lander.

2.3. Spacecraft Mathematical Model with Propellant Sloshing

The spacecraft model consists of a cubic rigid body, with a spherical propellant tank, and four landing legs, as shown in Fig. 8. Two reference frames are defined; the inertial frame C_N and the lander body fixed frame C_B. The inertial frame C_N corresponds the celestial body surface.

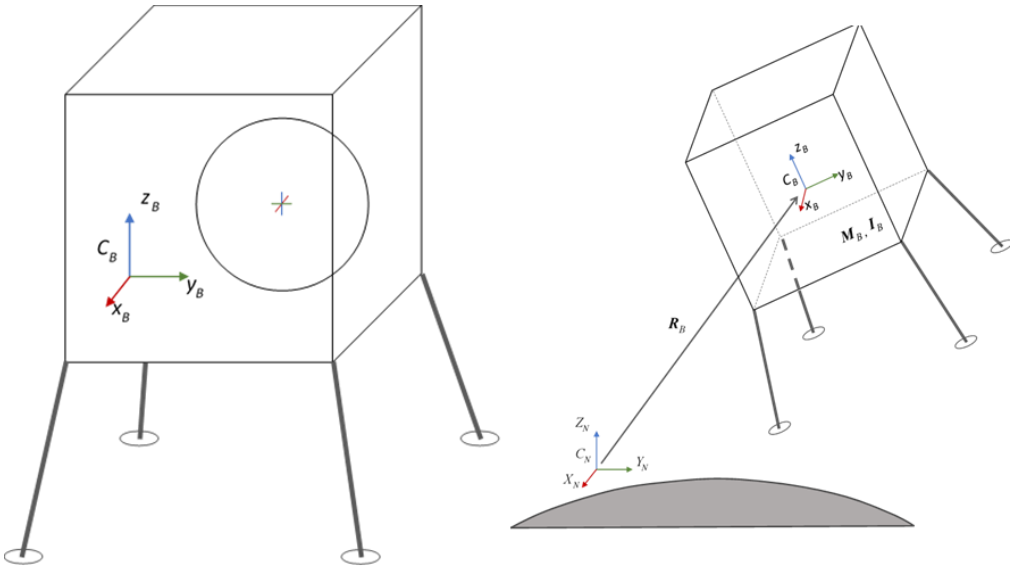

Figure 8: Celestial body lander model.

Vector $\boldsymbol{R}_B$ represents the position vector of the lander with respect to the inertial frame. M_B and I_B are the mass matrix and the moment of inertia matrix of the lander, respectively. The rigid body translational equation of motion is given by,

$$M_B\ddot{\boldsymbol{R}}_B = \boldsymbol{F}_T + \boldsymbol{F}_S + M_B\boldsymbol{g} \tag{17}$$

And the rotational equation of motion is defined using Euler's rotation equation as,

$$[J_B]\dot{\boldsymbol{\omega}} = -[\tilde{\omega}][J_B]\boldsymbol{\omega} + \boldsymbol{L}_T + \boldsymbol{L}_S \tag{18}$$

where $\boldsymbol{F}_S$ and $\boldsymbol{L}_S$ are the sloshing forces and torques. $\boldsymbol{F}_T$ and $\boldsymbol{L}_T$ are the touchdown forces and torques due to the impact with celestial body surface, the derivation of the touchdown forces and torques are detailed in section 2.4. Vector $\boldsymbol{\omega}$ represents the angular velocity of the lander with respect to the inertial frame. The tilde operator, $[\tilde{}]$, corresponds to the skew symmetric matrix defined as,

$$[\widetilde{\omega}] = \begin{bmatrix} 0 & -\omega_3 & \omega_2 \\ \omega_3 & 0 & -\omega_1 \\ -\omega_2 & \omega_1 & 0 \end{bmatrix}. \tag{19}$$

The attitude of the lander rigid body in the inertial frame is described using a unit quaternion defined as,

$$q = [q_0, q_1, q_2, q_3]^T \tag{20}$$

where q_0 is the scalar component of the quaternion and $[q_1, q_2, q_3]$ is the vector component. The differential kinematic equation of the unit quaternion is given as,

$$\dot{q} = \frac{1}{2}[B(q)]\omega \tag{21}$$

$$[B(q)] = \begin{bmatrix} -q_1 & -q_2 & -q_3 \\ q_0 & -q_3 & q_2 \\ q_3 & q_0 & -q_1 \\ -q_2 & q_1 & q_0 \end{bmatrix}$$

The mathematical model of the system is represented in algebraic form as,

$$\dot{x} = f(x)$$

$$x = [\boldsymbol{R}_b, \dot{\boldsymbol{R}}_b, \boldsymbol{q}, \boldsymbol{\omega}, \boldsymbol{P}_s, \dot{\boldsymbol{P}}_s, \boldsymbol{S}_{fp1}, \dot{\boldsymbol{S}}_{fp1}, \boldsymbol{S}_{fp2}, \dot{\boldsymbol{S}}_{fp2}, \boldsymbol{S}_{fp3}, \dot{\boldsymbol{S}}_{fp3}, \boldsymbol{S}_{fp4}, \dot{\boldsymbol{S}}_{fp4}]^T$$

where $\boldsymbol{R}_b$ is the position of the lander in inertial frame, $\boldsymbol{q}$ is the quaternion representation of the lander attitude, $\boldsymbol{\omega}$ is the angular velocity of the lander with respect to inertial frame, $\boldsymbol{P}_s$ is the position vector of the sloshing mass in the tank, $\boldsymbol{S}_{fpi}$ are the position vectors of the footpads with respect to the lander. The algebraic differential equation is solved using a 4th order Runge-Kutta solver in MATLAB software.

2.4. Interaction with the Celestial Body Surface

There are several theories regarding the properties of a celestial body surface, but it is not possible to know the actual properties without reaching the surface. If the surface is covered with regolith, then it is considered safer for landing because the presence of regolith provides

further damping action upon landing. On the other hand, little or no damping action occurs in the case of a rigid surface and there is a high possibility of rebound. To model the surface of the celestial body, a spring damper system is used, see Fig. 9. Soft and rigid ground conditions are simulated by changing the spring and damper coefficient values.

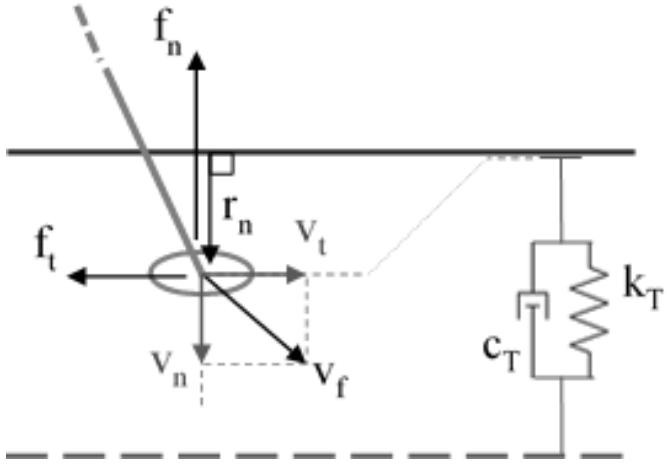

Figure 9: Celestial body surface interaction model.

The touchdown forces and torques are computed for each leg separately. For each leg, the impact force acting on the footpad is obtained from the penetration vector $\boldsymbol{r}_n$ and the velocity vector component normal to the surface, $\boldsymbol{v}_n$, of the footpad. The normal force component is obtained as,

$$\boldsymbol{f}_n = \begin{cases} 0 & ; \quad \boldsymbol{r}_n \geq 0 \\ -k_T \boldsymbol{r}_n - c_T \boldsymbol{v}_n & ; \quad \boldsymbol{r}_n < 0 \end{cases} \tag{22}$$

the tangential force component is obtained as,

$$\boldsymbol{f}_t = -|\mu \boldsymbol{f}_n| \frac{\boldsymbol{v}_t}{|\boldsymbol{v}_t|} \tag{23}$$

where $\boldsymbol{v}_t$ is the velocity vector component tangent to the surface and the constant μ is the coefficient of friction. The total touchdown force on each foot pad is obtained as,

$$\boldsymbol{F}_T = \boldsymbol{f}_n + \boldsymbol{f}_t \, . \tag{24}$$

Note that this force does not transfer directly to the lander rigid body due to the presence of the landing gear (spring-damper system) between the foot pad and the rigid body. The motion of the footpad is limited to linear motion along the leg direction vector $\hat{\boldsymbol{r}}_l$, see Fig. 10.

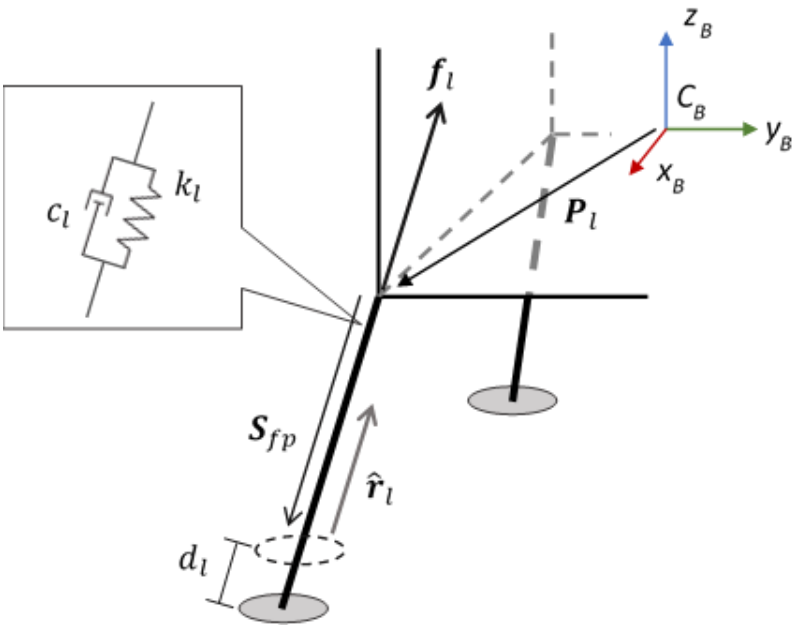

Figure 10: Landing gear dynamics

The touchdown force acting on the footpad is split into 2 components, a component along leg direction vector $\hat{\boldsymbol{r}}_l$ computed using the dot product as,

$$\boldsymbol{f}_{Tt} = (\boldsymbol{F}_T \cdot \hat{\boldsymbol{r}}_l)\hat{\boldsymbol{r}}_l \tag{25}$$

and a component perpendicular to the leg direction vector $\hat{\boldsymbol{r}}_l$ computed using the cross product as,

$$\boldsymbol{f}_{Tn} = \boldsymbol{F}_T \times \hat{\boldsymbol{r}}_l \tag{26}$$

the equation of motion of the footpad is given as,

$$m_{fp}\boldsymbol{S}_{fp} = \left(k_l d_l + c_l \dot{d}_l\right)\hat{\boldsymbol{r}}_l + \boldsymbol{F}_{Tt}$$

where $\boldsymbol{S}_{fp}$ is the position vector of the footpad with respect to leg attachment point, and d_l is the displacement of the footpad form it resting position, d_l is positive in the direction to extend

the leg. The force acting on the lander rigid body from the landing gear of each leg is computed as,

$$\boldsymbol{f}_l = \left(-k_l d_l - c_l \dot{d}_l\right)\hat{\boldsymbol{r}}_l \tag{27}$$

the torque acting on the lander rigid body from each leg is computed as,

$$\boldsymbol{l}_l = (\boldsymbol{P}_l \times \boldsymbol{f}_l) + [(\boldsymbol{P}_l + \boldsymbol{S}_{fp}) \times \boldsymbol{f}_{Tn}] \tag{28}$$

The total touchdown forces and torques acting on the rigid body from all four landing legs are computed as,

$$\boldsymbol{F}_l = \sum_{i=1}^{4} \boldsymbol{f}_{li} \tag{29}$$

$$\boldsymbol{L}_l = \sum_{i=1}^{4} \boldsymbol{l}_{li} \tag{30}$$

3. Lander Modelling and Simulations

3.1. Simulations Overview

The system's equations of motion are expressed as an algebraic differential equation and solved using a 4th order Runge-Kutta solver of the form:

$$\dot{X} = F(X,t) \quad ; \quad h: step\ size$$

$$K_1 = h * F(X_n, t_n)$$

$$K_2 = h * F(X_n + \frac{K_1}{2}, t_n + \frac{h}{2})$$

$$K_3 = h * F(X_n + \frac{K_2}{2}, t_n + \frac{h}{2})$$

$$K_4 = h * F(X_n + K_3, t_n + h)$$

$$X_{n+1} = X_n + \frac{1}{6}(K_1 + 2K_2 + 2K_3 + K_4) \tag{31}$$

All simulations were carried out using MATLAB software. Although the lander is modelled as a 3-dimensional structure, to simplify the analysis, the motion is considered in one plane only. The simulations are divided into two main cases; low gravity simulations and high gravity simulations. For each case several landing scenarios are simulated with and without the presence of propellant sloshing and the dynamic behavior of the lander is analyzed to study the effects of propellant sloshing.

3.2. Low Gravity Simulations

3.2.1. Overview

In low gravity conditions the effects of surface tension are dominant and the liquid spreads along the wall of the tank in steady state, when the spacecraft is subjected to a large acceleration,

as in the moment of touchdown, the propellant shifts and concentrates on one side of the tank and is forced into sloshing motion. This is modelled using a 3-dimesional rotating mass-spring-damper system as shown in Fig. 11. The details of the model are presented in section 2.2.

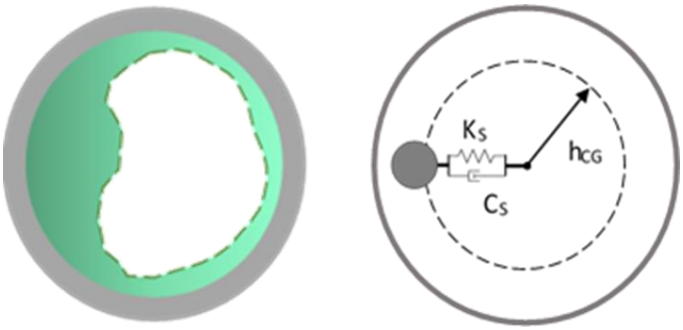

Figure 11: Low gravity propellant sloshing model.

Several simulations were conducted to study the effects of large amplitude propellant sloshing on the lander dynamics and examine how these effects change under different system configurations. It is assumed that the lander is in a free fall situation and the only forces and torques acting on the lander are from gravity, sloshing, and touchdown. The lander is modelled as a cubic rigid body with a spherical tank at an arbitrary location, figure 12 shows a 2D front view of the lander.

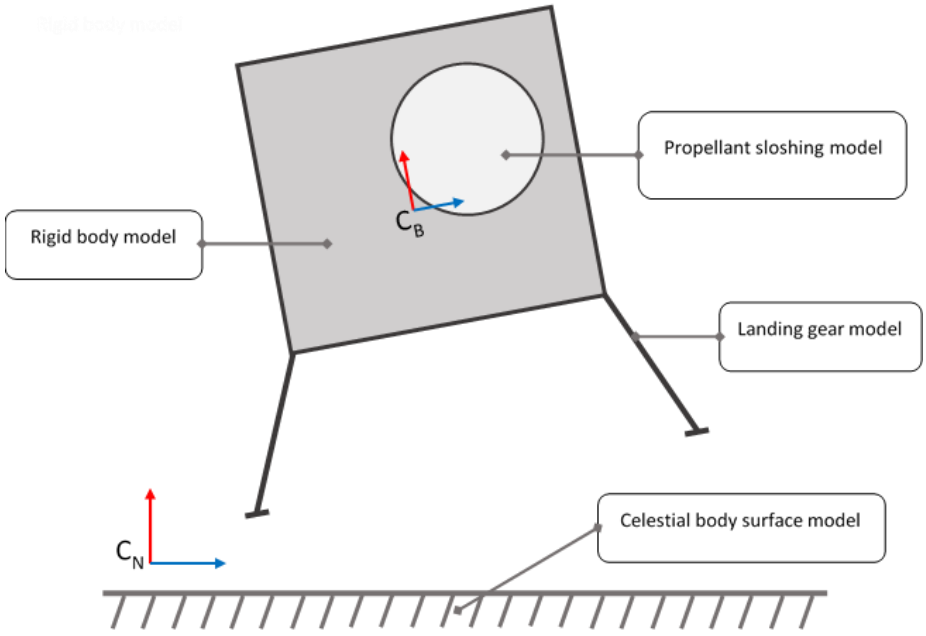

Figure 12: 2D front view of lander

Simulations are divided into 2 parts, in part I the effects of propellant sloshing are studied for different landing situations. part II examines how these effects vary under for different system configurations. The simulation parameters are summarized in table 1.

Table 1: Low gravity simulation parameters

Parameter	Value	Unit
Dry body mass	600	kg
Sloshing propellant mass	350	kg
Slosh natural frequency	5.0	Hz
Tank radius	0.5	m
Surface spring constant	100	kN/m
Surface damping coefficient	0.1	kNs/m
Landing gear spring constant	1.0	kN/m
Landing gear damping coefficient	0.5	kNs/m

Part I: 2 high-risk landing situations are considered, A - Lateral Descent, B - Inclined Surface. As previously mentioned, the tank is assumed to be arbitrarily located which means that the lander is not necessarily symmetric. Therefore, for situation A (lateral descent), simulations are done twice, each with different velocity direction. Similarly, for situation B (inclined surface), simulations are done twice, each with different inclination direction. Figure 13 illustrates part I simulations.

Part 2: 2 factors are considered in these simulations; tank location dependency and lander with multiple tanks. To examine how the effects of propellant sloshing change for different tank locations we consider 3 cases. In the first case the tank position only has a horizontal displacement with respect to the lander center of mass, in the second case the tank position only has a vertical displacement, in the third case the tank location has a vertical and horizontal displacements, the 3 cases are illustrated in Fig. 14. The same simulations from part I are conducted for the 3 cases. To examine the effect of sloshing on a lander with multiple tanks, the same simulations are conducted for a lander with 2 tanks positioned symmetrically about the lander center of mass.

3.2.2. Simulation and Results

Part I

Effects of propellant sloshing are studied for different landing situations. The landing situations are illustrated in Figure 13.

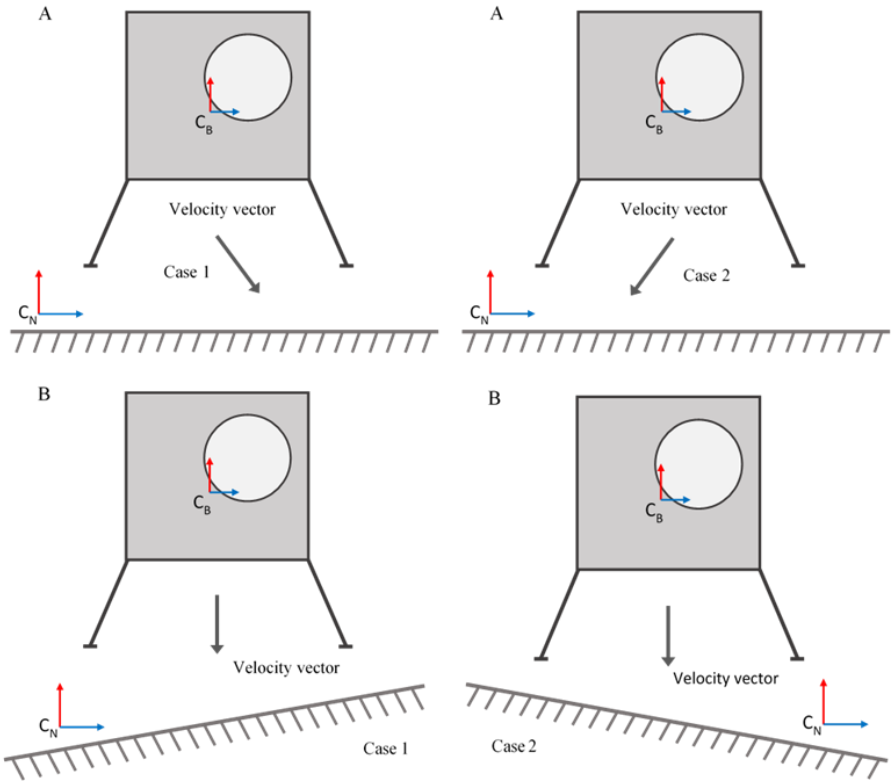

Figure 13: low gravity simulations overview

A. Lateral descent

In case of descending with a lateral velocity component, the impact with the surface can cause the lander's angular velocity to accelerate which can cause the lander to tip over or start tumbling. This simulation investigates how the lander's behavior is affected by the presence of propellant sloshing. As previously mentioned, because the tank location is assumed to be arbitrary with respect to the lander center of mass, the lander is not necessarily symmetric in structure, two cases are considered, each with opposite lateral velocity directions.

Case 1:

For case 1, the lander has a lateral velocity in the positive y-axis direction. Figures 14 (a) and (b) show the simulations overview with and without the presence of propellant sloshing,

respectively. Figures 14 (c) and (f) show the position and attitude displacement of the lander with and without propellant sloshing, respectively. Figures 14 (d) and (g) show the linear and angular velocity of the lander with and without propellant sloshing, respectively. Figures 14 (e) and (h) show the total angular momentum of the lander with and without propellant sloshing, respectively.

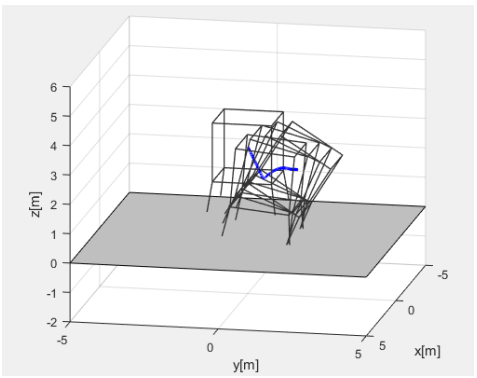

a) Overview (w/o sloshing)

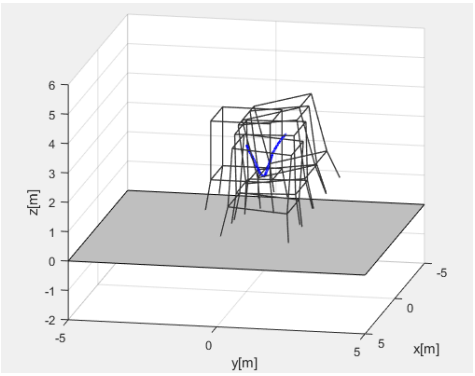

b) Overview (w/ sloshing)

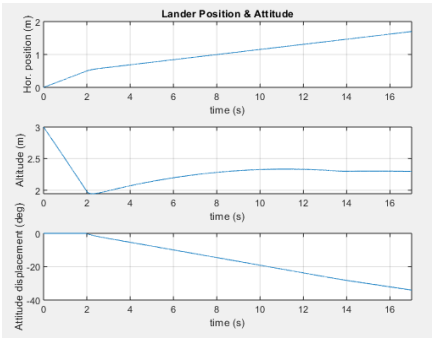

c) Position & Attitude (w/o sloshing)

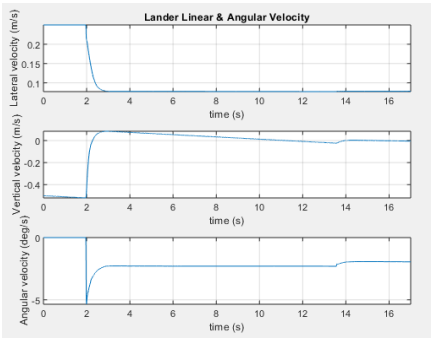

d) Lin. & Ang. velocity (w/o sloshing)

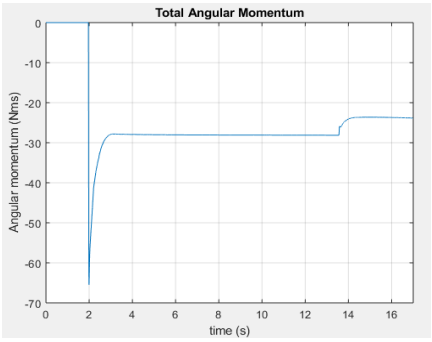

e) Ang. momentum (w/o sloshing)

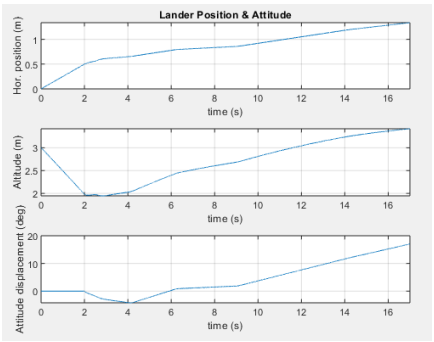

f) Position & Attitude (w/ sloshing)

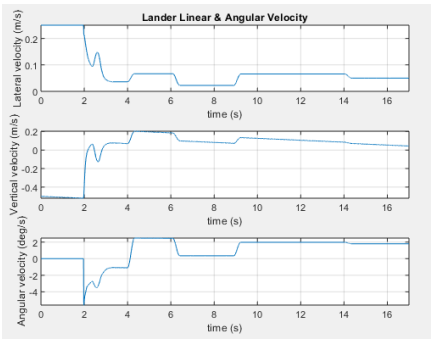

g) Lin. & Ang. velocity (w/ sloshing)

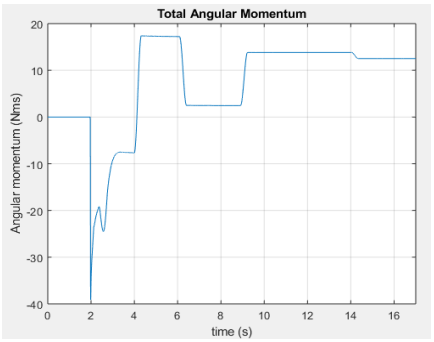

h) Ang. momentum (w/ sloshing)

Figure 14: Lateral descent case 1 simulation results with and without sloshing (lateral velocity = 0.25 m/s)

For the case of lateral descent in the positive y-axis direction, the simulation results show that propellant sloshing has a significant impact on the behavior of the lander at touchdown. With respect to the attitude displacement, propellant sloshing causes the lander to tumble in the opposite direction compared to the case without sloshing. It also increases the vertical velocity of the lander after rebound causing the lander to reach higher altitudes. Moreover, the presence of propellant sloshing causes fluctuations in the angular momentum of the lander which can be harmful as it might excite oscillations of other flexible components of the lander such as solar panels. Table 2 summarizes the key parameter values of the simulation, note that the maximum angular velocity magnitude in the presence of sloshing is higher, and there is a significant difference in the average angular velocity of the lander after rebound. There is also a notable increase in the maximum vertical velocity of the lander.

Table 2: Low gravity lateral descent 1 simulation results summary.

Parameter	w/o Sloshing	w/ Sloshing	unit
Max angular velocity mag.	5.36	5.61	deg/s
Avg. angular velocity	-2.26	1.13	deg/s
Max vertical velocity	0.08	0.20	m/s
Avg. vertical velocity	0.02	0.09	m/s

Case 2:

For case 2, the lander has a lateral velocity in the negative y-axis direction. Figures 15 (a) and (b) show the simulations overview with and without the presence of propellant sloshing, respectively. Figures 15 (c) and (f) show the position and attitude displacement of the lander with and without propellant sloshing, respectively. Figures 15 (d) and (g) show the linear and angular velocity of the lander with and without propellant sloshing, respectively. Figures 15 (e) and (h) show the total angular momentum of the lander with and without propellant sloshing, respectively.

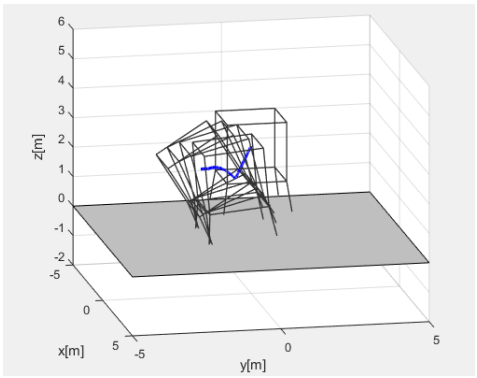

a) Overview (w/o sloshing)

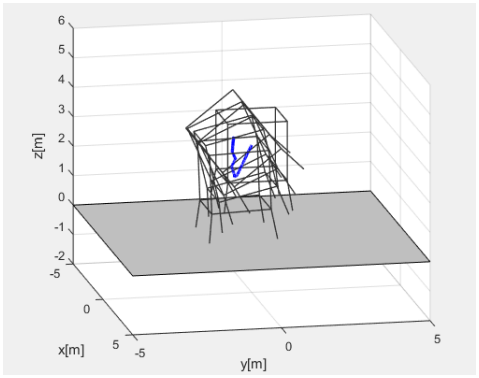

b) Overview (w/ sloshing)

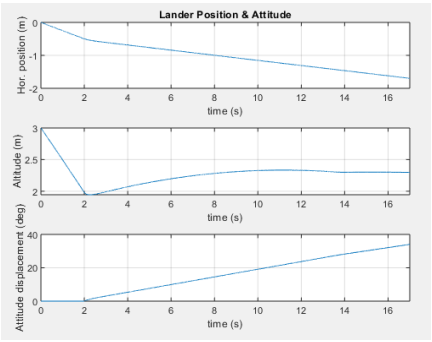

c) Position & Attitude (w/o sloshing)

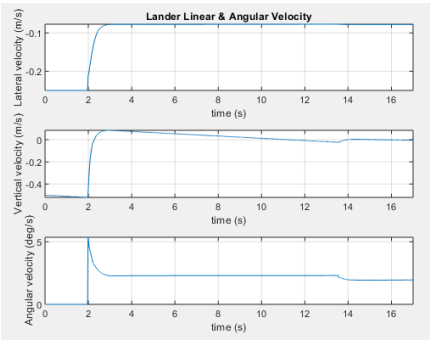

d) Lin. & Ang. velocity (w/o sloshing)

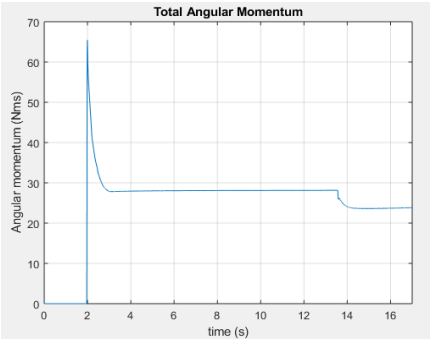

e) Ang. momentum (w/o sloshing)

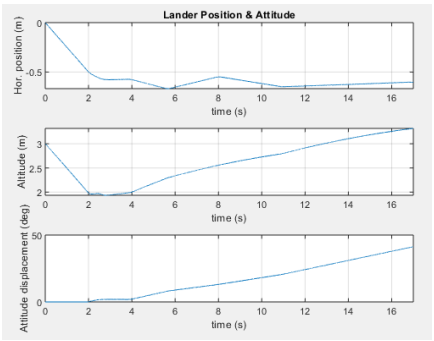

f) Position & Attitude (w/ sloshing)

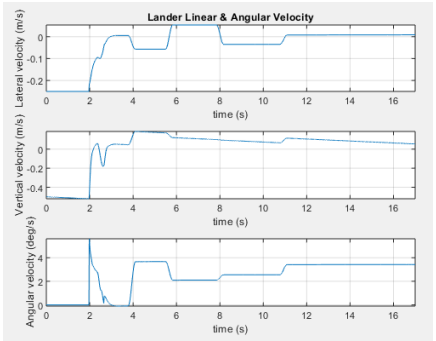

g) Lin. & Ang. velocity (w/ sloshing)

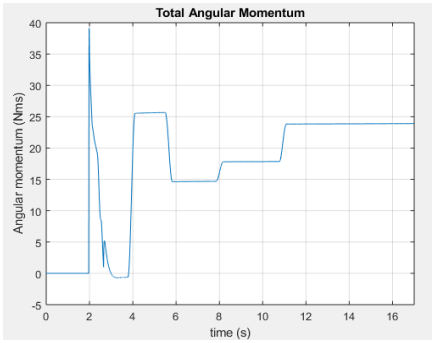

h) Ang. momentum (w/ sloshing)

Figure 15: Lateral descent case 2 simulation results with and without sloshing (lateral velocity = 0.25 m/s)

For the case of lateral descent in the negative y-axis direction, the simulation results show that the effect of propellant sloshing is not as significant as in the previous case. Propellant sloshing causes a slight increase in the angular velocity of the lander after rebound causing a small increase in the attitude displacement of the lander. A significant increase can be seen in the altitude of the lander after rebound due to the higher rebound velocity caused by propellant sloshing. As in the previous case the presence of propellant sloshing causes fluctuations in the angular momentum of the lander which can be harmful as it might excite oscillations of other

flexible components of the lander such as solar panels. Table 3 summarizes the key parameter values of the simulation, as shown both the maximum angular velocity magnitude and the average angular velocity of the lander are higher in the presence of sloshing. In addition, there is a significant increase in the maximum vertical velocity of the lander.

Table 3: Low gravity lateral descent 2 simulation results summary.

Parameter	w/o Sloshing	w/ Sloshing	unit
Max angular velocity mag.	5.36	5.61	deg/s
Avg. angular velocity	2.26	2.75	deg/s
Max vertical velocity	0.08	0.19	m/s
Avg. vertical velocity	0.02	0.09	m/s

B. Inclined surface

More often than not, the terrain is characterized by rough surface, irregular structures, and slopes, which makes it more difficult to maintain the stability of the lander a touchdown. Therefore, this simulation examines the effect of propellant sloshing on the lander in case of a touchdown on an inclined terrain. As in the lateral descent simulations, because the lander is not necessarily symmetric in structure, two cases are considered each with opposite direction of inclination.

Case 1:

For case 1,the surface is inclined in the counterclockwise direction about the x-axis. Figures 16 (a) and (b) show the simulations overview with and without the presence of propellant sloshing, respectively. Figures 16 (c) and (f) show the position and attitude displacement of the lander with and without propellant sloshing, respectively. Figures 16 (d) and (g) show the linear and angular velocity of the lander with and without propellant sloshing, respectively. Figures 16 (e) and (h) show the total angular momentum of the lander with and without propellant sloshing, respectively.

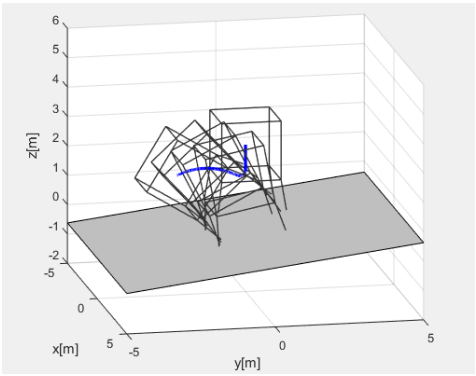

a) Overview (w/o sloshing)

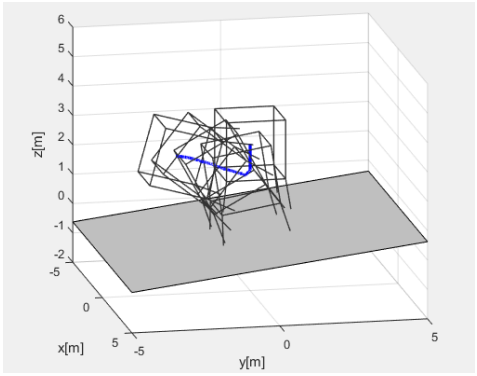

b) Overview (w/ sloshing)

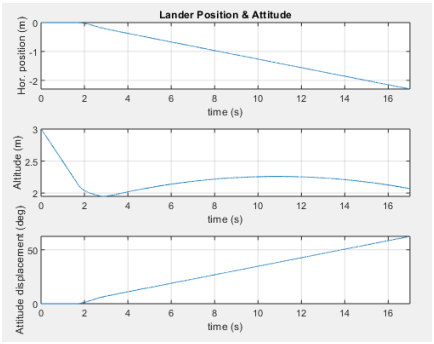

c) Position & Attitude (w/o sloshing)

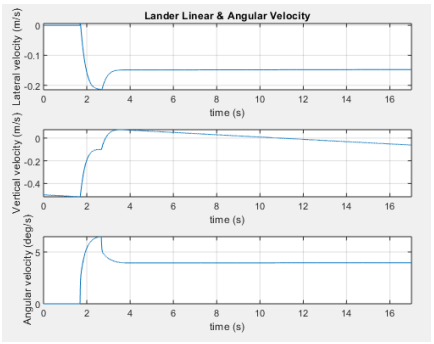

d) Lin. & Ang. velocity (w/o sloshing)

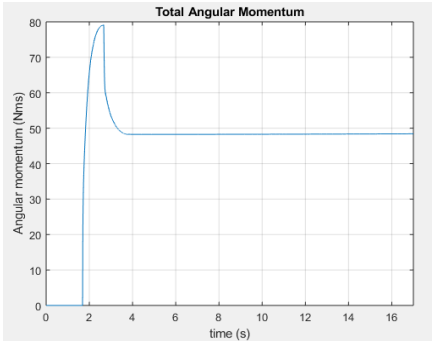

e) Ang. momentum (w/o sloshing)

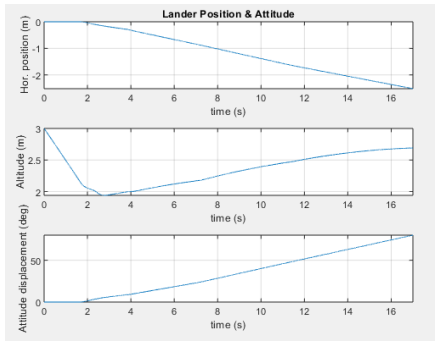

f) Position & Attitude (w/ sloshing)

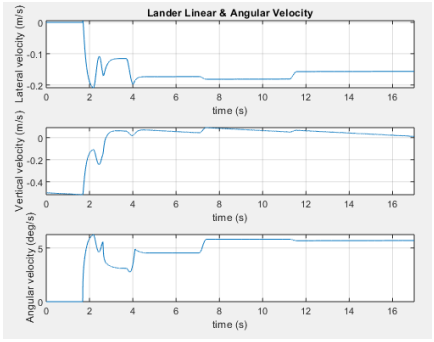

g) Lin. & Ang. velocity (w/ sloshing)

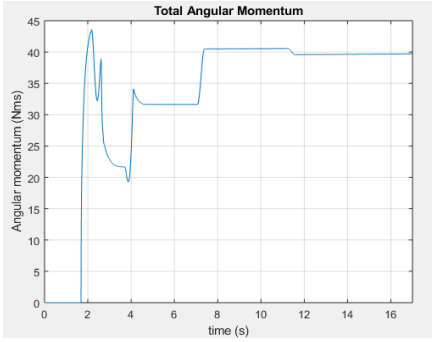

h) Ang. momentum (w/ sloshing)

Figure 16: Inclined surface case 1 simulation results with and without sloshing (inclination angle = 10 deg)

For the case of an inclined surface in the counterclockwise direction, the simulation results show that propellant sloshing has a notable impact on the behavior of the lander at touchdown. With respect to the attitude displacement, propellant sloshing causes a higher angular velocity of the lander resulting in a larger attitude displacement. An increase in the vertical velocity of the lander after rebound can be seen causing the lander to reach higher altitudes. Additionally, propellant sloshing results in fluctuations in the angular momentum of the lander which can be harmful as it might excite oscillations of other flexible components of the lander such as solar

panels. Table 4 summarizes the key parameter values of the simulation, note that in the presence of sloshing the maximum angular velocity magnitude is smaller, but the average angular velocity of the lander is higher.

Table 4: Low gravity inclined surface 1 simulation results summary.

Parameter	w/o Sloshing	w/ Sloshing	unit
Max angular velocity mag.	6.48	6.24	deg/s
Avg. angular velocity	4.08	5.22	deg/s
Max vertical velocity	0.07	0.09	m/s
Avg. vertical velocity	0.0	0.04	m/s

Case 2:

For case 2,the surface is inclined in the clockwise direction about the x-axis. Figures 17 (a) and (b) show the simulations overview with and without the presence of propellant sloshing, respectively. Figures 17 (c) and (f) show the position and attitude displacement of the lander with and without propellant sloshing, respectively. Figures 17 (d) and (g) show the linear and angular velocity of the lander with and without propellant sloshing, respectively. Figures 17 (e) and (h) show the total angular momentum of the lander with and without propellant sloshing, respectively.

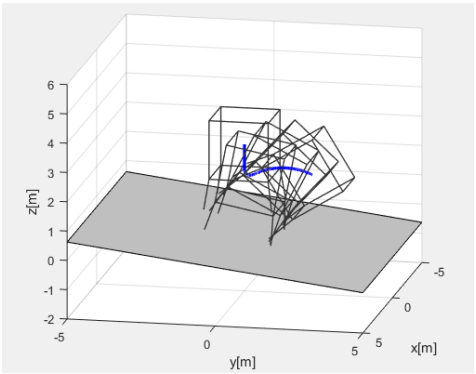

a) Overview (w/o sloshing)

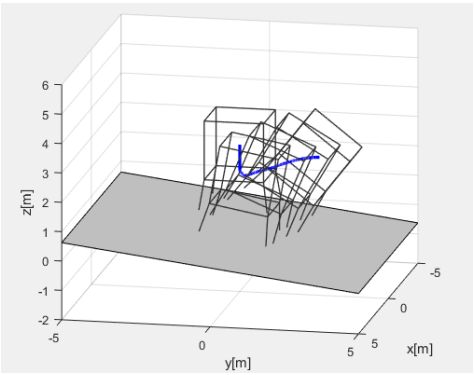

b) Overview (w/ sloshing)

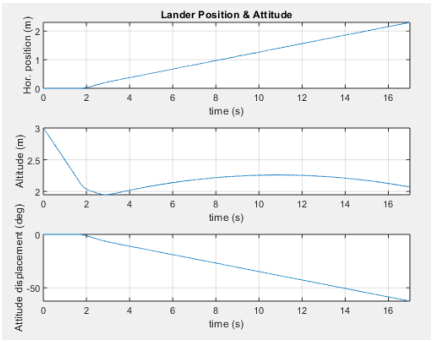

c) Position & Attitude (w/o sloshing)

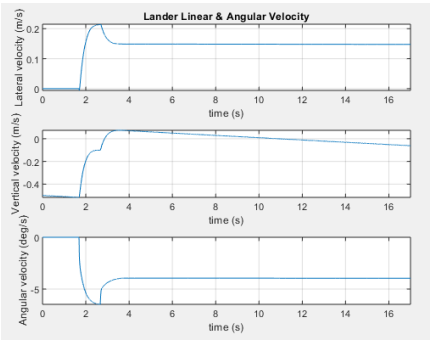

d) Lin. & Ang. velocity (w/o sloshing)

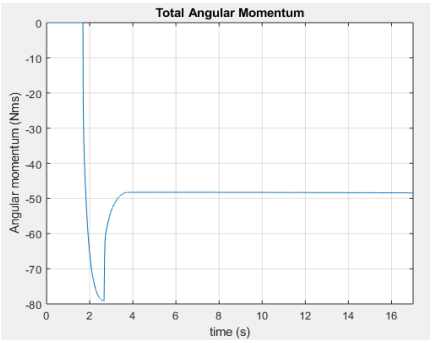

e) Ang. momentum (w/o sloshing)

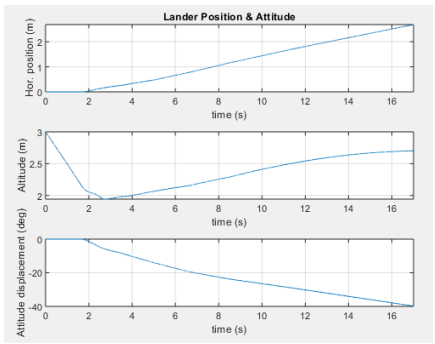

f) Position & Attitude (w/ sloshing)

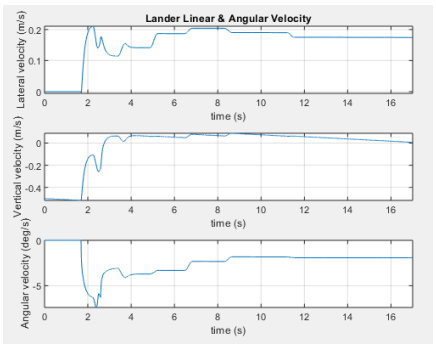

g) Lin. & Ang. velocity (w/ sloshing)

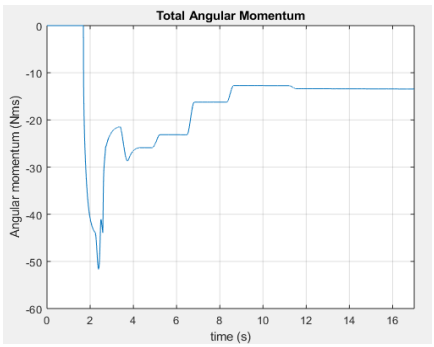

h) Ang. momentum (w/ sloshing)

Figure 17: Inclined surface case 2 simulation results with and without sloshing (inclination angle = 10 deg)

For the case of an inclined surface in the clockwise direction, it can be seen that propellant sloshing has a positive effect on the attitude displacement of the lander, sloshing provides a damping effect on the angular velocity of the lander after rebound. A small increase in the vertical velocity of the lander can be seen. As in the previous case, fluctuations in the angular momentum of the lander are caused by sloshing which can be harmful as it might excite oscillations of other flexible components of the lander such as solar panels. Table 5 summarizes the key parameter values of the simulation. As shown, in the presence of sloshing the lander records a higher maximum angular velocity magnitude, but there is a significant decrease in the average angular velocity value.

Table 5: Low gravity inclined surface 2 simulation results summary.

Parameter	w/o Sloshing	w/ Sloshing	unit
Max angular velocity mag.	6.48	7.4	deg/s
Avg. angular velocity	-4.08	-2.60	deg/s
Max vertical velocity	0.07	0.09	m/s
Avg. vertical velocity	0.0	0.04	m/s

Part II

Tank location dependency

The torques acting on the lander body from propellant sloshing are directly related to the position of the tank. In the simulations presented previously, the tank is positioned with a horizontal displacement along the y-axis only with respect to the lander center of mass, shown as case 1 in Fig. 18. In this section, 2 more cases for the tank position are considered, tank position with vertical displacement only, and tank position with both vertical and horizontal displacement, shown as cases 2 and 3 in Fig. 18, respectively. The same landing simulations from part I are conducted for the 2 cases, and the simulations results for the 3 tank position cases are compared.

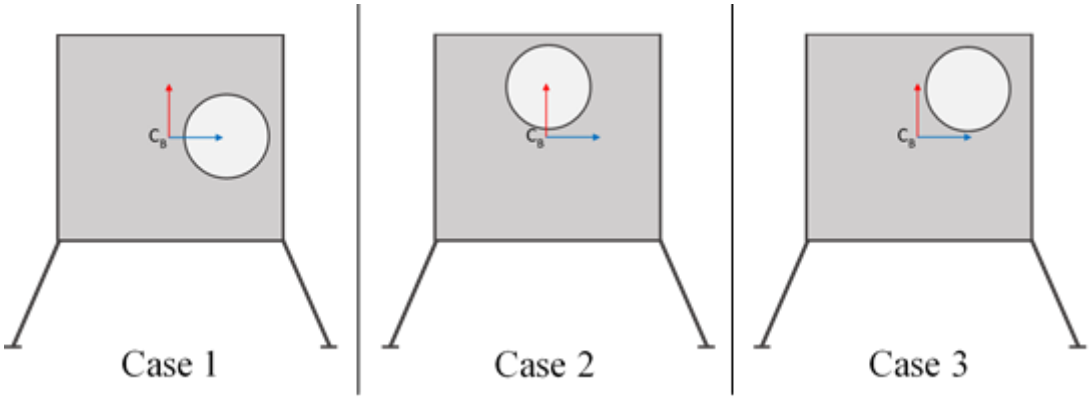

Figure 18: Tank location dependency simulations overview

A. Lateral descent

For the lateral descent simulations, a lateral velocity in the positive y-axis direction is considered. The simulation results for the 3 tank positions are presented in Fig. 19. Figures 19 (a), (d) and (g) show the position and attitude displacement of the lander for tank positions 1, 2 and 3, respectively. Figures 19 (b), (e) and (h) show the linear and angular velocity of the lander for tank positions 1, 2 and 3, respectively. Figures 19 (c), (f) and (i) show the total angular momentum of the lander for tank positions 1, 2 and 3, respectively.

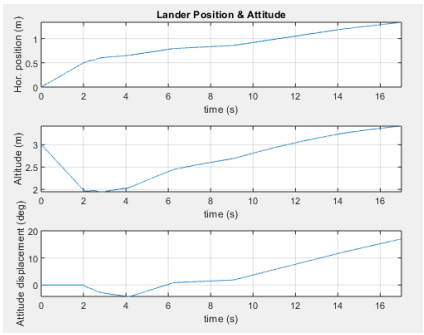

a) Position & Attitude (Case 1)

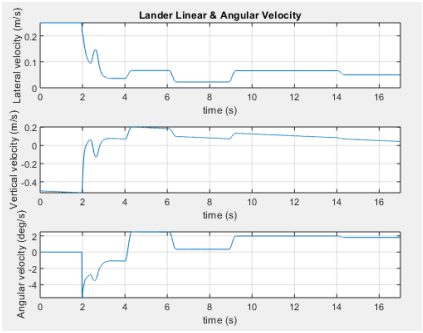

b) Lin. & Ang. velocity (Case 1)

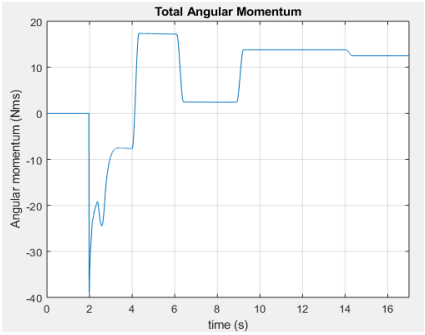

c) Ang. momentum (Case 1)

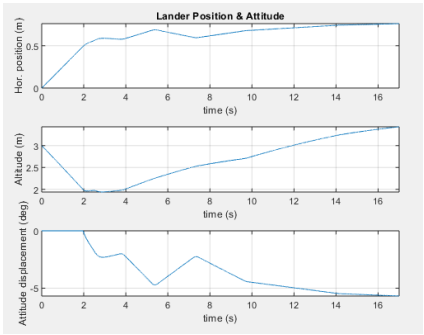

d) Position & Attitude (Case 2)

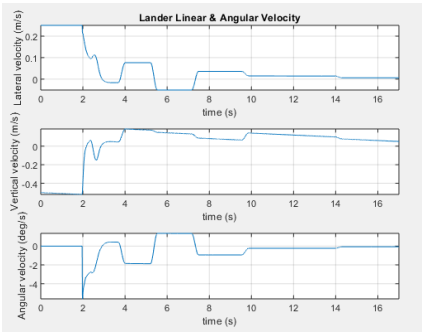

e) Lin. & Ang. velocity (Case 2)

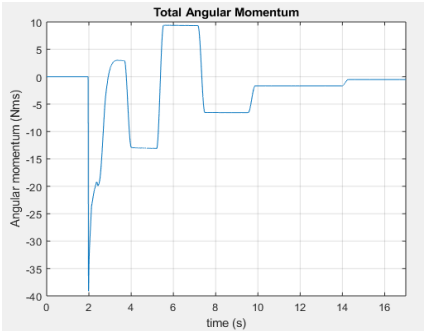

f) Ang. momentum (Case 2)

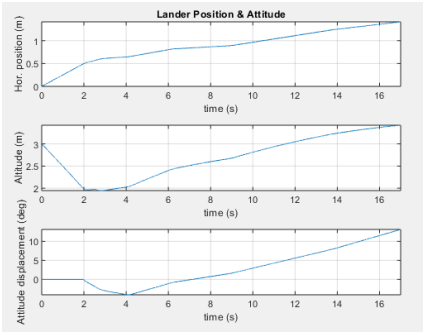

g) Position & Attitude (Case 3)

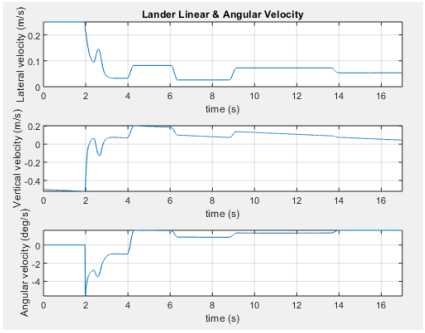

h) Lin. & Ang. velocity (Case 3)

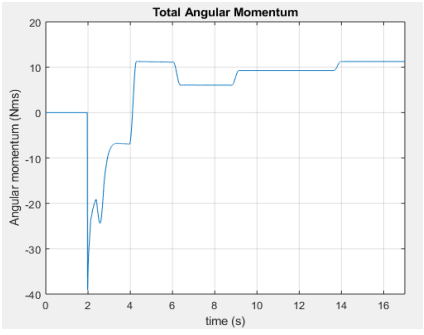

i) Ang. momentum (Case 3)

Figure 19: Tank location dependency lateral descent simulation results (lateral velocity = 0.25 m/s)

For the case of lateral descent, the simulation results show significant differences in the behavior of the lander depending on the position of the tank with respect to the lander center of mass. The results show that a tank position with vertical displacement only (case 2) results in better lander behavior after rebound, sloshing provides significant damping effect on the angular velocity of the lander causing minimal attitude displacement.

B. Inclined surface

For the inclined surface simulations, a clockwise inclination about the x-axis is considered. The simulation results for the 3 tank positions are presented in Fig. 20. Figures 20 (a), (d) and (g) show the position and attitude displacement of the lander for tank positions 1, 2 and 3, respectively. Figures 20 (b), (e) and (h) show the linear and angular velocity of the lander for tank positions 1, 2 and 3, respectively. Figures 20 (c), (f) and (i) show the total angular momentum of the lander for tank positions 1, 2 and 3, respectively.

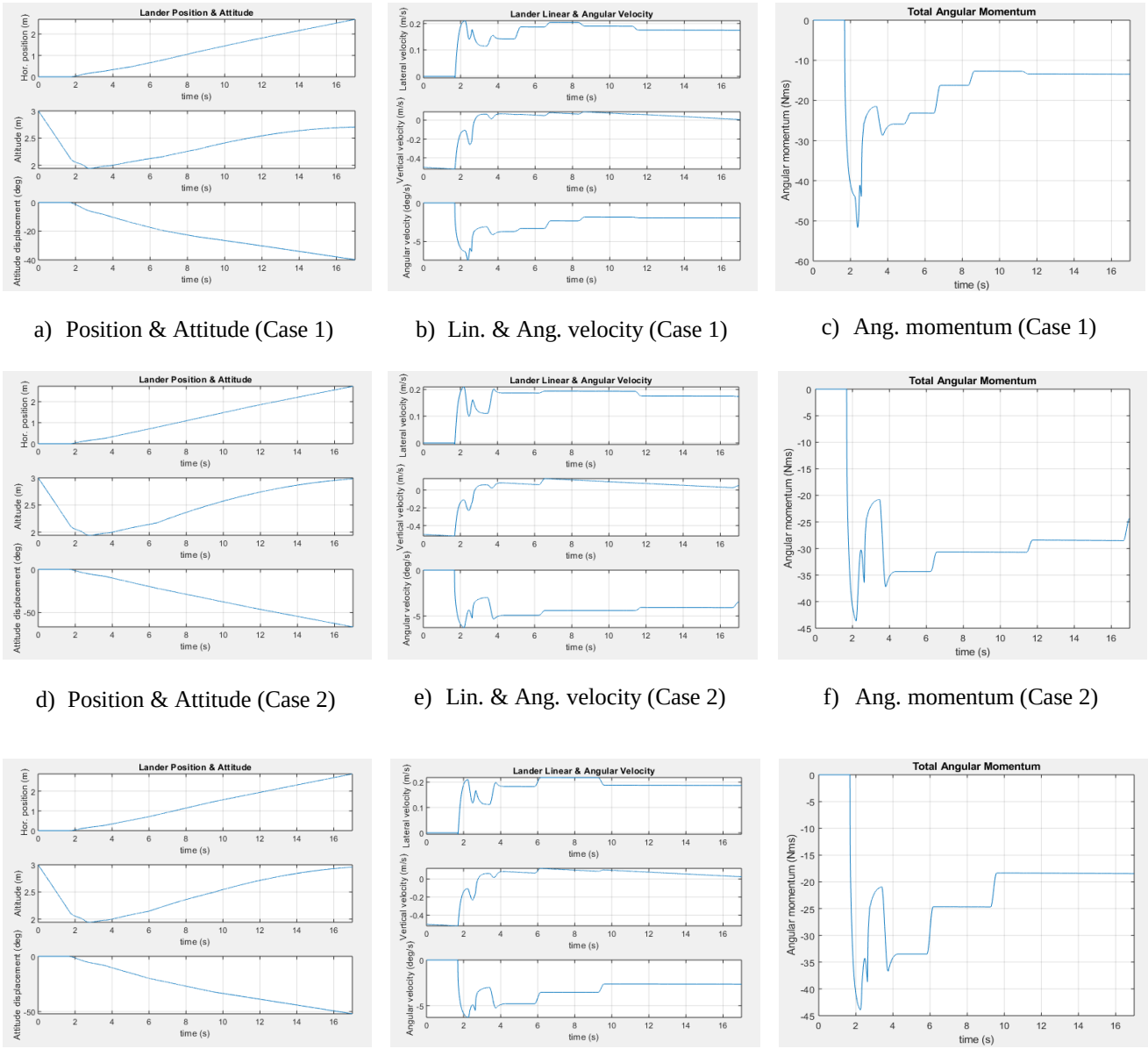

a) Position & Attitude (Case 1) b) Lin. & Ang. velocity (Case 1) c) Ang. momentum (Case 1)

d) Position & Attitude (Case 2) e) Lin. & Ang. velocity (Case 2) f) Ang. momentum (Case 2)

g) Position & Attitude (Case 3) h) Lin. & Ang. velocity (Case 3) i) Ang. momentum (Case 3)

Figure 20: Tank location dependency inclined surface simulation results (inclination angle = 10 deg)

For the case of landing on an inclined surface, the simulation results show notable differences in the behavior of the lander depending on the position of the tank with respect to the lander center of mass. The results show that a tank position with a horizontal displacement only (case 1) results in a smaller attitude displacement of the lander and smaller vertical velocity after rebound.

Multiple tanks

So far, the simulations were done for a lander with one spherical tank (one propellant sloshing EMM). However, in many cases, spacecrafts are equipped with multiple propellant tanks, therefore in this section landing simulations are conducted for a lander with 2 spherical tanks (2 propellant sloshing EMMs), the tanks are positioned such that the lander is symmetric in the y-z plane, as illustrated in Fig. 21. Two landing situations are simulated, lateral descent and inclined surface, for each simulation 3 cases are considered, first case is without sloshing, second case assumes the initial states of the propellant sloshing models for each tank are identical, third case assumes non-identical initial states of the propellant sloshing models.

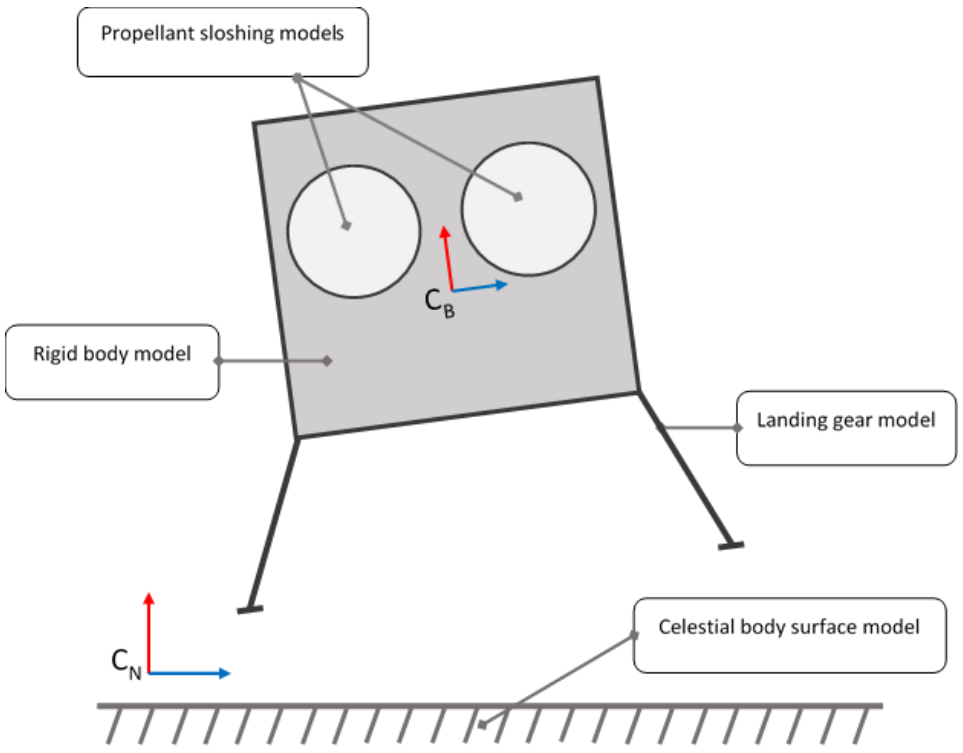

Figure 21: Lander model with multiple tanks

A. Lateral descent

The simulation results for the 3 cases are presented in Fig. 22. Figures 22 (a), (d) and (g) show the position and attitude displacement of the lander for cases 1, 2 and 3, respectively. Figures 22 (b), (e) and (h) show the linear and angular velocity of the lander for cases 1, 2 and 3, respectively. Figures 22 (c), (f) and (i) show the total angular momentum of the lander for cases 1, 2 and 3, respectively.

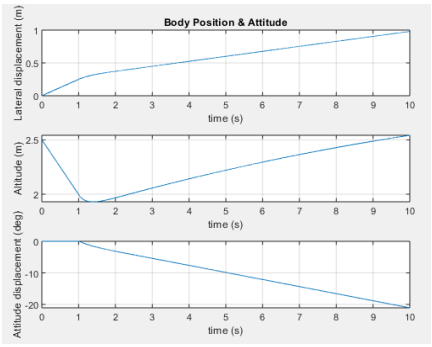

a) Position & Attitude (w/o sloshing)

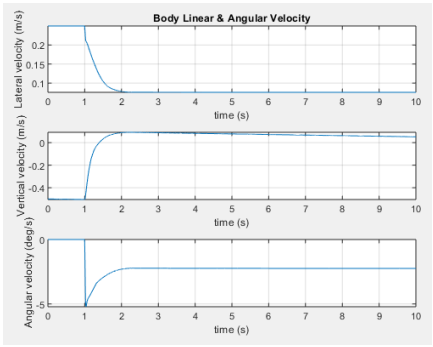

b) Lin. & Ang. velocity (w/o sloshing)

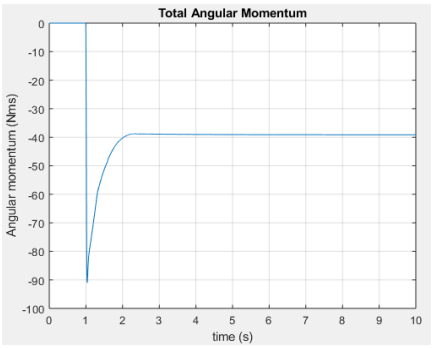

c) Ang. momentum (w/o sloshing)

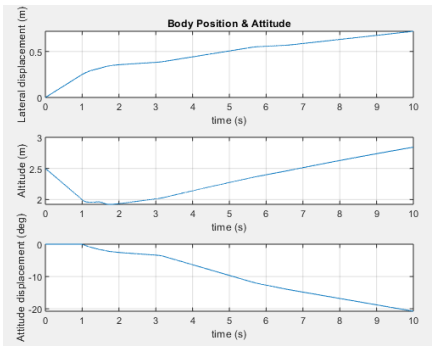

d) Position & Attitude (identical)

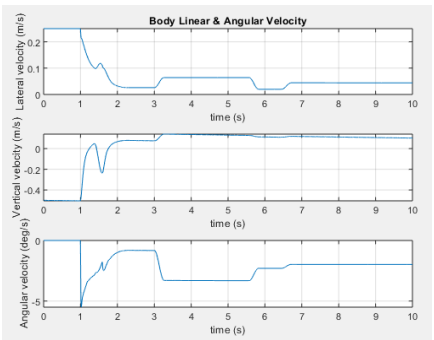

e) Lin. & Ang. velocity (identical)

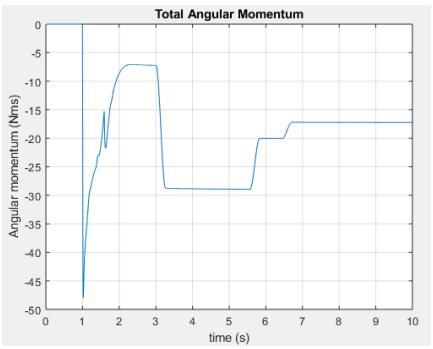

f) Ang. momentum (identical)

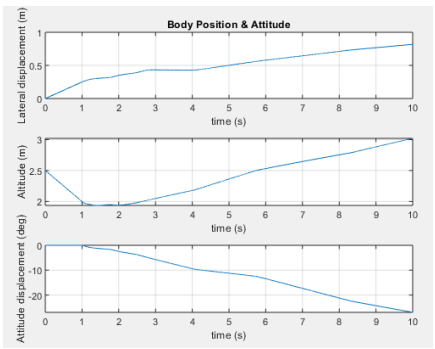

g) Position & Attitude (nonidentical)

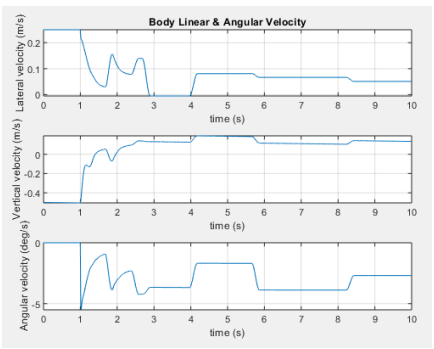

h) Lin. & Ang. velocity (nonidentical)

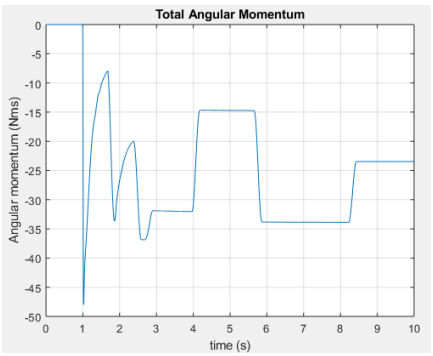

i) Ang. momentum (nonidentical)

Figure 22: Multiple tanks lateral descent simulation results (lateral velocity = 0.25 m/s)

The simulation results show that in the case of identical initial states, sloshing has no significant effect on the lander attitude, but there is an increase in vertical and lateral displacements after rebound. However, in the case of non-identical initial states of sloshing models, the lander has a larger attitude displacement and larger linear displacement. Moreover, a lander with multiple tanks shows larger changes in the angular momentum. Table 6 summarizes the key parameters of the simulation. As shown, a lander with sloshing models of non-identical initial states records notably larger maximum angular velocity and average angular velocity, and larger maximum and average vertical velocity after rebound.

Table 6: Multiple tanks lateral descent simulation results summary

Parameter	w/o Sloshing	w/ Sloshing (Identical)	w/ Sloshing (Nonidentical)	unit
Max angular velocity mag.	5.21	5.49	5.52	deg/s
Avg. angular velocity	-2.34	-2.31	-3.01	deg/s
Max vertical velocity	0.10	0.14	0.19	m/s
Avg. vertical velocity	0.06	0.09	0.11	m/s

B. Inclined surface

The simulation results for the 3 cases are presented in Fig. 23. Figures 23 (a), (d) and (g) show the position and attitude displacement of the lander for cases 1, 2 and 3, respectively. Figures 23 (b), (e) and (h) show the linear and angular velocity of the lander for cases 1, 2 and 3, respectively. Figures 23 (c), (f) and (i) show the total angular momentum of the lander for cases 1, 2 and 3, respectively.

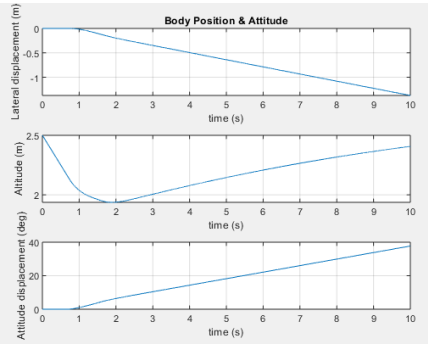

a) Position & Attitude (w/o sloshing)

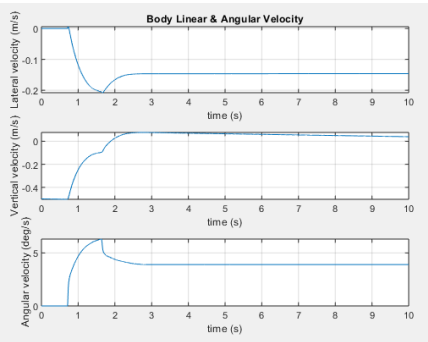

b) Lin. & Ang. velocity (w/o sloshing)

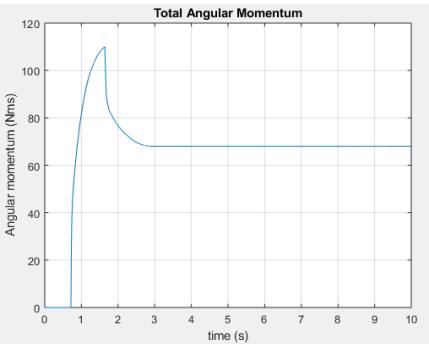

c) Ang. momentum (w/o sloshing)

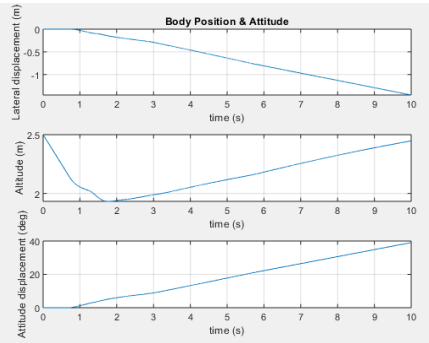

d) Position & Attitude (identical)

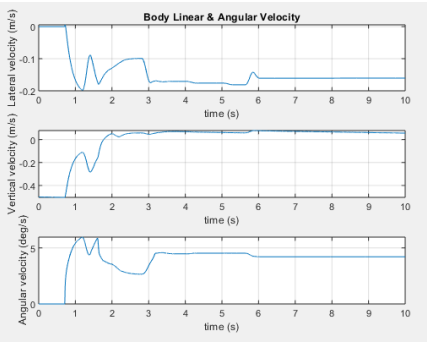

e) Lin. & Ang. velocity (identical)

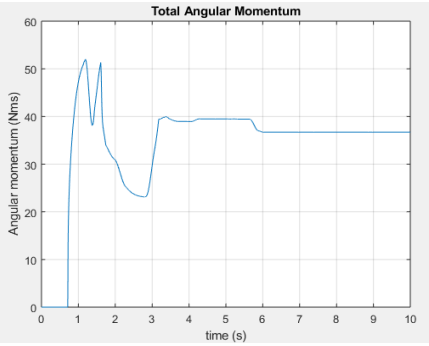

f) Ang. momentum (identical)

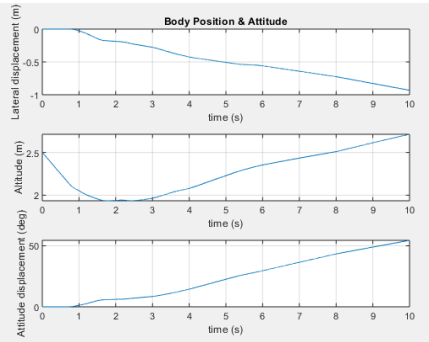

g) Position & Attitude (nonidentical)

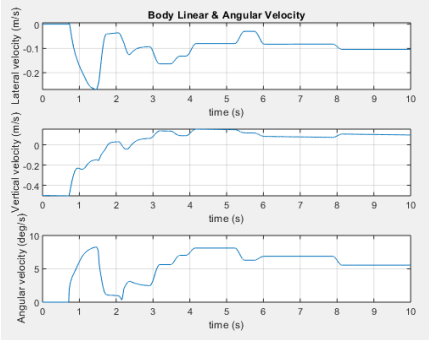

h) Lin. & Ang. velocity (nonidentical)

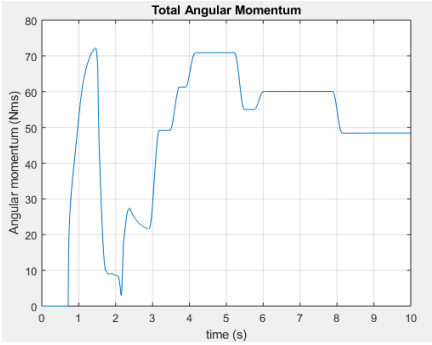

i) Ang. momentum (nonidentical)

Figure 23: Multiple tanks inclined surface simulation results (inclination angle = 10 deg)

As in the previous simulation, the results show that in the case of identical initial states, sloshing has no significant effect on the lander dynamics after rebound. However, in the case of non-identical initial states of sloshing models, the lander has a larger attitude displacement and larger linear displacement. Table 7 summarizes the key parameters of the simulation. As shown, in the case of sloshing models of non-identical initial states, there is a significant increase in the maximum angular velocity and average angular velocity of the lander, and larger maximum and average vertical velocity after rebound.

Table 7: Multiple tanks inclined surface simulation results summary

Parameter	w/o Sloshing	w/ Sloshing (Identical)	w/ Sloshing (Nonidentical)	unit
Max angular velocity mag.	6.30	5.61	8.28	deg/s
Avg. angular velocity	4.05	4.20	5.86	deg/s
Max vertical velocity	0.08	0.08	0.15	m/s
Avg. vertical velocity	0.03	0.03	0.06	m/s

3.3. High Gravity Simulations

3.3.1. Overview

In the case of landing on large bodies with significant gravity constant, gravitational forces are dominant over capillary forces and the propellant concentrates on one side of the tank in steady state. When the lander is subjected to a disturbance, as in the moment of touchdown, sloshing occurs at the free surface of the propellant within the tank. Although several sloshing modes can occur at the free surface, lateral sloshing has the most significant effects and therefore will be considered for high gravity simulations. Lateral sloshing is modelled using a linear mass-spring-damper system as shown in Fig. 24. The details of the model are presented in section 2.2.

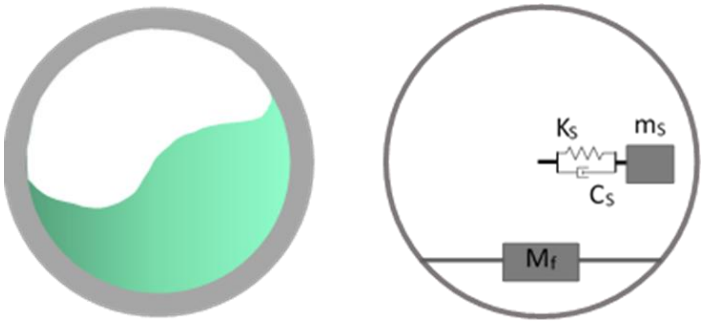

Figure 24: High gravity propellant sloshing model.

Several landing simulations were conducted to study the effects of lateral sloshing on lander dynamics and stability. Two landing scenarios where considered, landing with lateral velocity and landing on an inclined surface, see Fig. 25.

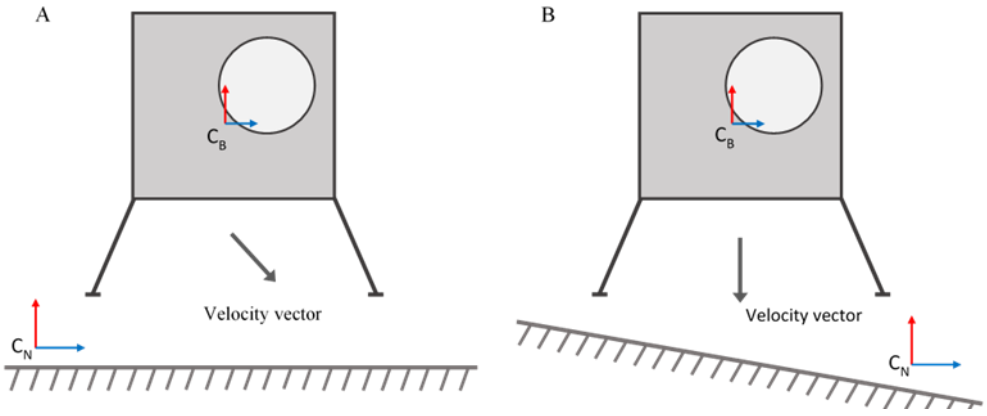

Figure 25: High gravity simulations overview.

For each scenario several simulations were conducted at different gravity constants with and without the presence of lateral sloshing, the dynamic behavior of the lander in both cases are examined and compared to study the effects of lateral sloshing on a lander under high gravity conditions. The simulations parameters are summarized in table 8.

Table 8: High gravity simulation parameters.

Parameter	Value	Unit
Dry body mass	600	kg
Sloshing propellant mass	100	kg
Slosh natural frequency	0.6	Hz
Tank radius	0.5	m
Surface spring constant	100	kN/m
Surface damping coefficient	0.1	kNs/m
Landing gear spring constant	1.0	kN/m
Landing gear damping coefficient	0.5	kNs/m

3.3.2. Simulation and Results

A. Lateral descent

A touchdown with a lateral velocity can result in a high risk of overturning, and in the presence of lateral sloshing the risk of overturning can increase. Therefore, several simulations are conducted at different values for the gravity constants with and without the presence of lateral sloshing. To evaluate the impact of lateral sloshing, for each gravity value the maximum stable lateral velocity is recorded with and without sloshing. The simulation results of lateral descent at a gravity constant of 1.0 m/s^2 are shown in Fig. 26. Figures 26 (a) and (b) show the landing simulations overview with and without sloshing, respectively. Figures 26 (c) and (d) show the attitude displacement of the lander with and without sloshing, respectively. Figures 26 (e) and (f) show the angular velocity of the lander with and without sloshing, respectively. Table 9 summarizes the maximum stable lateral velocities the lander can have before overturning for different gravity constants with and without the presence of lateral sloshing.

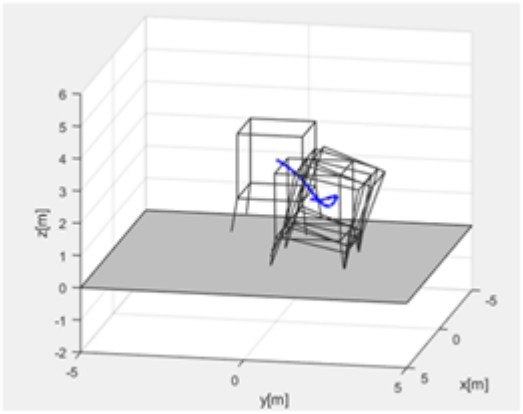

a) Overview (w/o sloshing)

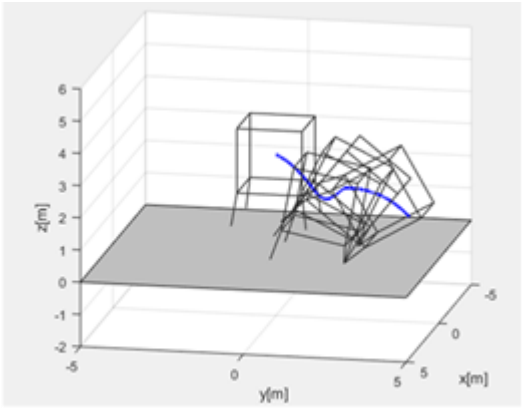

b) Overview (w/ sloshing)

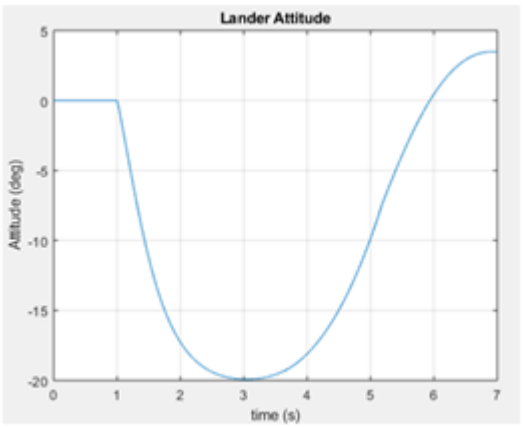

c) Attitude displacement (w/o sloshing)

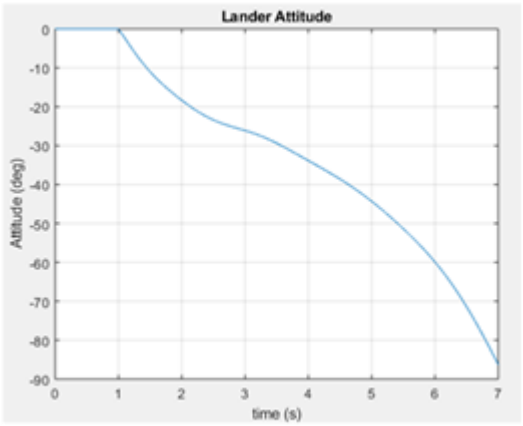

d) Attitude displacement (w/ sloshing)

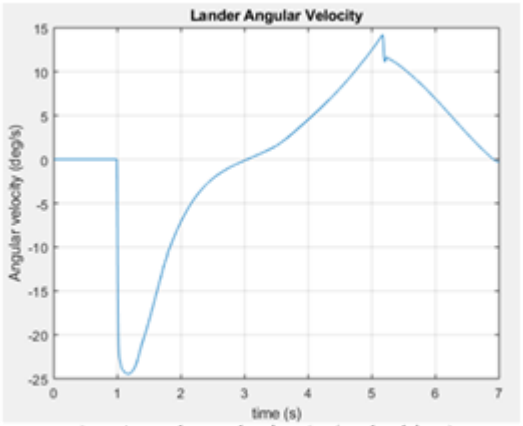

e) Angular velocity (w/o sloshing)

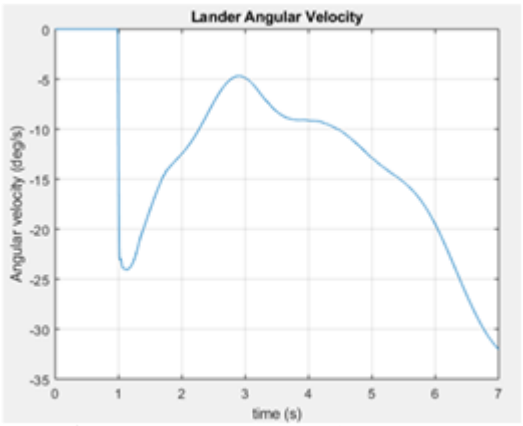

f) Angular velocity (w/ sloshing)

Figure 26: High gravity lateral descent simulation results with and without sloshing (gravity constant = 1.0 m/s^2, lateral velocity = 1.15 m/s)

The simulation results reveal that the presence of lateral sloshing can have a notable effect on the stability of a lander approaching the surface with lateral velocity. As shown in table 7, for each gravity value the maximum stable lateral velocity is smaller in the presence of sloshing.

Moreover, as the value of the gravity constant increases, the effect of sloshing on the stability of the lander becomes more apparent, as evident by the increase in the difference of the maximum stable velocity with and without sloshing as gravity increases.

Table 9: Maximum stable lateral velocity under high gravity w/ and w/o sloshing for different gravity constants

Gravity constant (m/s^2)	Maximum stable lateral velocity (m/s)		Difference (m/s)
	W/O Sloshing	W/ Sloshing	
0.5	0.99	0.77	0.22
0.75	1.16	0.91	0.25
1.0	1.29	1.02	0.27
1.25	1.41	1.11	0.30
1.5	1.51	1.19	0.32

B. Inclined surface

A touchdown on an inclined surface is one of the most high-risk situations a lander can encounter, and in the presence of lateral sloshing the risk can increase. Therefore, several simulations are conducted at different values for the gravity constants with and without the presence of lateral sloshing. The simulation results of landing on an inclined surface at a gravity constant of 1.0 m/s^2 with and without lateral sloshing are shown in Fig. 27. Figures 27 (a) and (b) show the landing simulation overview with and without sloshing, respectively. Figures 27 (c) and (d) show the attitude displacement of the lander with and without sloshing, respectively. Figures 27 (e) and (f) show the angular velocity of the lander with and without sloshing, respectively. Table 10 summarizes the maximum stable surface inclination the lander can perform a touchdown on before overturning for different gravity constants with and without the presence of lateral sloshing.

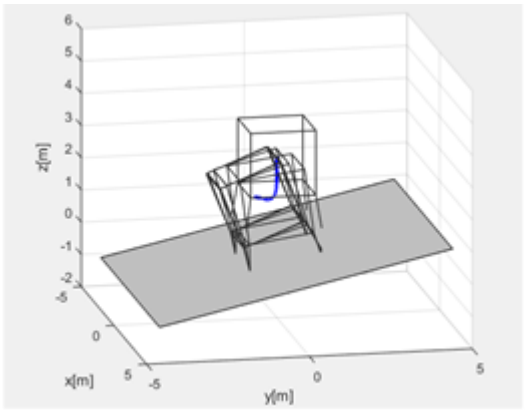

a) Overview (w/o sloshing)

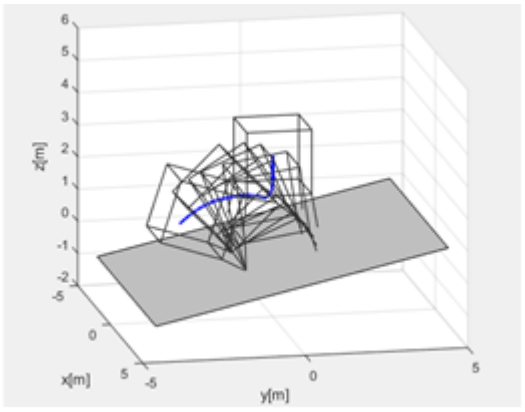

b) Overview (w/ sloshing)

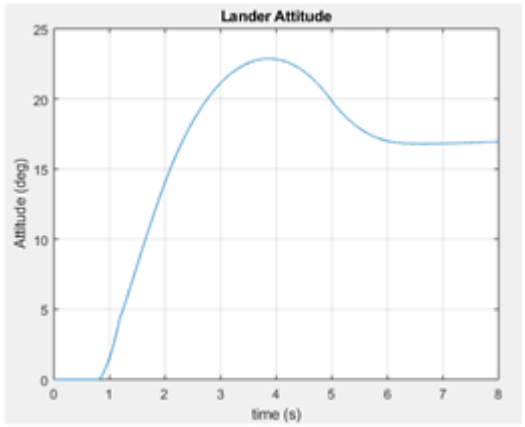

c) Attitude displacement (w/o sloshing)

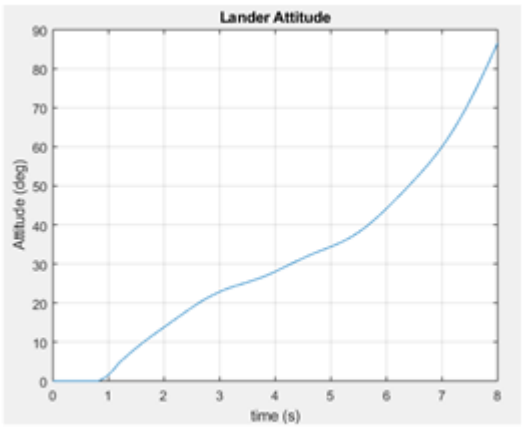

d) Attitude displacement (w/ sloshing)

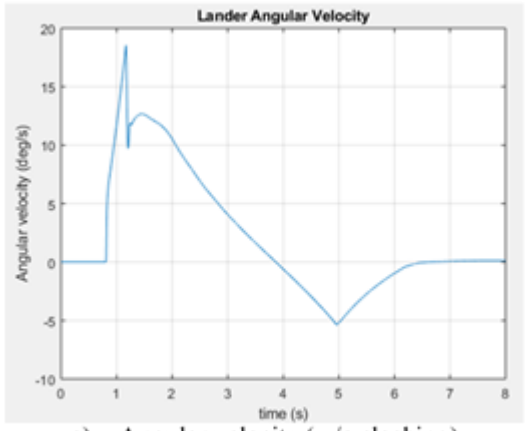

e) Angular velocity (w/o sloshing)

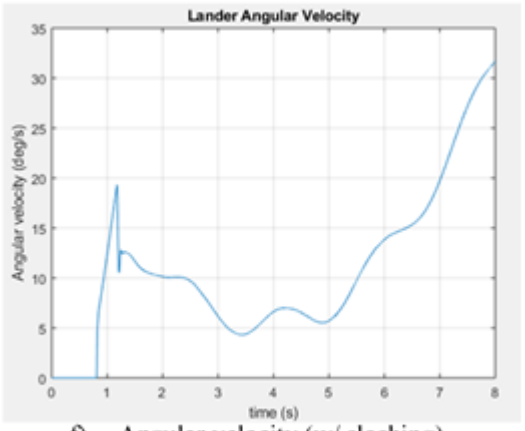

f) Angular velocity (w/ sloshing)

Figure 27: High gravity inclined surface simulation results with and without sloshing (gravity constant = 1.0 m/s^2, inclination angle = 13 deg)

For the case of landing on an inclined surface, the simulation results show that lateral sloshing can have a notable effect on the stability of the lander. As shown in table 8, for each gravity value the maximum stable inclination angle is smaller in the presence of sloshing. In

addition, note that as the value of the gravity constant increases, the effect of sloshing on the stability of the lander becomes more apparent, as evident by the increase in the difference of the maximum stable inclination angle with and without sloshing as gravity increases.

Table 10: Maximum stable inclination under high gravity w/ and w/o sloshing for different gravity constants

Gravity constant (m/s^2)	Maximum stable Inclination (deg)		Difference (deg)
	W/O Sloshing	W/ Sloshing	
0.5	11.53	9.46	2.07
0.75	12.65	10.49	2.16
1.0	13.78	11.53	2.25
1.25	14.38	12.01	2.37
1.5	14.74	12.26	2.48

4. Variable Landing Gear for Lander Stabilization

4.1. Concept

The most interesting regions of planets, moons, and natural satellites are often the most challenging to access. Such regions include crater central hills, lunar lava tubes, highlands and canyons, which hold valuable data of high scientific value. However, these regions often feature challenging terrain with rough surface conditions, many slopes, and obstacle such as rocks. Achieving a successful touchdown on these regions requires a landing gear that can adapt to the different surface conditions that can be present.

Different surface conditions require different landing gears, horizontal flat surfaces require soft landing gears, rough surfaces or slopes require more stiff landing gears to support the attitude of the spacecraft. Passive landing gears are designed to satisfy the stabilization requirements for specific cases, which can be unfeasible for other cases. To optimize all of the performance parameters simultaneously and satisfy the conflicting requirements, Maeda, T. et. al. proposed the use of a variable damper landing gear. Controlling the damping coefficient of each landing gear of the spacecraft allows the landing system to adapt to the complex surface conditions. A large damping coefficient supports the attitude of the spacecraft and prevents the acceleration of angular velocity. On the other hand, a small damping coefficient provide higher shock absorption for the landing leg that first touches the surface [36].

In their paper, several landing simulations are presented to validate the performance of the variable damper landing gears. The simulations included landing on an inclined surface and landing with lateral velocity, in both cases the results showed that the variable damper landing gear provided higher stability than the passive landing gear. However, in the simulations the lander is considered as a simple rigid body with no flexible components, and the presence of large disturbances such as propellant sloshing is not considered. In this section, the validity and

performance of the variable damper landing gear is examined in the presence of a significant disturbance such as propellant sloshing.

4.2. Control law derivation

As in the case of high gravity lander simulations, the lander is modelled as a cubic rigid body with four landing legs and a spherical tank. Landing gears are modelled as spring-damper systems and lateral sloshing is modelled using a linear mass-spring-damper system, the lander model is depicted in Fig. 28.

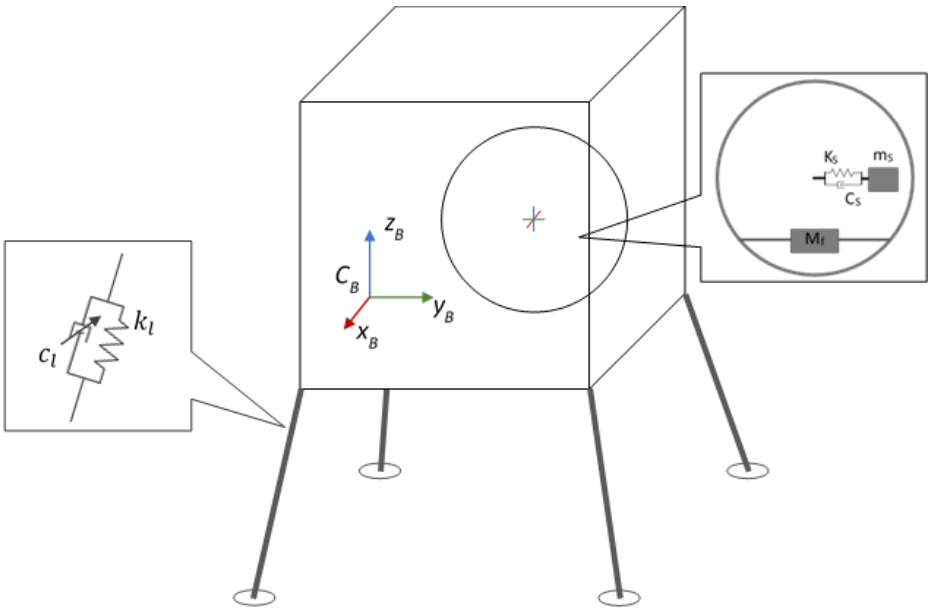

Figure 28: Lander model with variable damper landing gear.

The rotational equation of motion of the lander body in three-dimensional space can be expressed as,

$$\boldsymbol{J}_b\dot{\boldsymbol{\omega}} = -[\tilde{\omega}]\boldsymbol{J}_b\boldsymbol{\omega} + \boldsymbol{L} \tag{32}$$

where $\boldsymbol{J}_b$ is the moment of inertia matrix of the lander body, $\boldsymbol{\omega}$ is the angular velocity vector of the lander body with respect to inertial frame, and $\boldsymbol{L}$ is the vector of torques acting on the body at touchdown. Vector $\boldsymbol{L}$ can be expressed as the sum of torques acting on the lander body from each landing gear as shown below.

$$\boldsymbol{L} = \sum_{i=1}^{4} \boldsymbol{\tau}_i \tag{34}$$

The torque $\boldsymbol{\tau}_i$ exerted on the body from landing gear i can be expressed in terms of the force exerted on the body from the landing gear, $\boldsymbol{f}_i$, and position vector of the point of application of the force, $\boldsymbol{r}_i$, see Fig. 29.

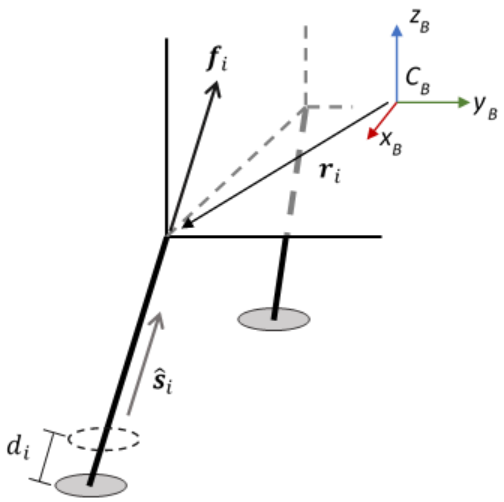

Figure 29: Landing gear force diagram

$$\boldsymbol{\tau}_i = [\tilde{r}_i]\boldsymbol{f}_i \tag{35}$$

To derive the control low of the variable damper landing gear, a Lyapunov function is chosen as,

$$V = \frac{1}{2}\boldsymbol{\omega}^T \boldsymbol{J}_b \boldsymbol{\omega} \tag{36}$$

and the time derivative of the Lyapunov function V is,

$$\dot{V} = \boldsymbol{\omega}^T \boldsymbol{J}_b \dot{\boldsymbol{\omega}} \tag{37}$$

Substituting for $\boldsymbol{J}_b\dot{\boldsymbol{\omega}}$ from Eq. 32 and for $\boldsymbol{\tau}_i$ from Eq. 34, the time derivative of the Lyapunov function becomes,

$$\dot{V} = \boldsymbol{\omega}^T(-[\tilde{\omega}]\boldsymbol{J}_b\boldsymbol{\omega} + [\tilde{r}_i]\boldsymbol{f}_i) \tag{38}$$

In matrix form the time derivative of the Lyapunov function is written as,

$$\dot{V} = [\omega_x \quad \omega_y \quad \omega_z]\left(-\begin{bmatrix} 0 & -\omega_z & \omega_y \\ \omega_z & 0 & -\omega_x \\ -\omega_y & \omega_x & 0 \end{bmatrix}\begin{bmatrix} J_x & 0 & 0 \\ 0 & J_y & 0 \\ 0 & 0 & J_z \end{bmatrix}\begin{bmatrix} \omega_x \\ \omega_y \\ \omega_z \end{bmatrix} + \begin{bmatrix} 0 & -r_{iz} & r_{iy} \\ r_{iz} & 0 & -r_{ix} \\ -r_{iy} & r_{ix} & 0 \end{bmatrix}\begin{bmatrix} f_{ix} \\ f_{iy} \\ f_{iz} \end{bmatrix}\right) \tag{39}$$

performing matrix multiplication, the time derivative expands to,

$$\dot{V} = [\omega_x \quad \omega_y \quad \omega_z]\left(-\begin{bmatrix} \omega_y\omega_z(-J_y + J_z) \\ \omega_x\omega_z(J_x - J_z) \\ \omega_x\omega_y(-J_x + J_y) \end{bmatrix} + \begin{bmatrix} -r_{iz}f_{iy} + r_{iy}f_{iz} \\ r_{iz}f_{ix} - r_{ix}f_{iz} \\ 0 \end{bmatrix}\right) \tag{40}$$

note that force $\boldsymbol{f}_i$ and position vector $\boldsymbol{r}_i$ lie on the same plane that is perpendicular to the x-y plane and therefore the third component of the cross product $\boldsymbol{r}_i \times \boldsymbol{f}_i$ is zero. Multiplying in the angular velocity, the time derivative expands to,

$$\dot{V} = \omega_x(-r_{iz}f_{iy} + r_{iy}f_{iz}) + \omega_y(r_{iz}f_{ix} - r_{ix}f_{iz}). \tag{41}$$

The landing gear force $\boldsymbol{f}_i$ can be expressed in terms of the direction vector of the landing leg, $\hat{\boldsymbol{s}}_i$, and the size of the landing gear force f_i.

$$\boldsymbol{f}_i = f_i\hat{\boldsymbol{s}}_i \tag{42}$$

Furthermore, the direction vector $\hat{\boldsymbol{s}}_i$ can be expressed in terms of the position vector $\boldsymbol{r}_i$ and constants β and γ as,

$$s_{ix} = -\beta r_{ix} \quad ; \quad s_{iy} = -\beta r_{iy} \quad ; \quad s_{iz} = -\gamma r_{iz} \tag{43}$$

constants β and γ are described as,

$$\beta = -\frac{s_{ix}r_{iy} + r_{ix}s_{iy}}{2r_{ix}r_{iy}} \quad ; \quad \gamma = -\frac{s_{iz}}{r_{iz}} \tag{44}$$

substituting Eq. 43 into Eq. 42, force $\boldsymbol{f}_i$ becomes,

$$\begin{bmatrix} f_{ix} \\ f_{iy} \\ f_{iz} \end{bmatrix} = \begin{bmatrix} -\beta f_i r_{ix} \\ -\beta f_i r_{iy} \\ -\gamma f_i r_{iz} \end{bmatrix}. \tag{45}$$

Note that all landing legs have the same value of β and γ. The time derivative of the Lyapunov function can be rewritten in terms of position vector $\boldsymbol{r}_i$ components and constants β and γ as shown below.

$$\begin{aligned}\dot{V} &= \omega_x\left(\beta f_i r_{iy} r_{iz} - \gamma f_i r_{iz} r_{iy}\right) + \omega_y(-\beta f_i r_{ix} r_{iz} + \gamma f_i r_{iz} r_{ix}) \\ &= \omega_x(\beta - \gamma) f_i r_{iy} r_{iz} + \omega_y(-\beta + \gamma) f_i r_{ix} r_{iz} \\ &= f_i r_{iz}(\beta - \gamma)(\omega_x r_{iy} - \omega_y r_{ix})\end{aligned} \tag{46}$$

Note that the landing legs are semi vertical with respect to the lander body frame, so γ is large compared to β. In the model shown in Fig. 27 r_{iz} and s_{iz} have opposite signs in the lander body frame, therefore if r_{iz} is positive, then γ is negative and vice versa. Consequently, the term $r_{iz}(\beta - \gamma)$ is always positive, and can be replaced by a positive constant α, the time derivative of the Lyapunov function becomes,

$$\dot{V} = f_i \alpha(\omega_x r_{iy} - \omega_y r_{ix}) \tag{47}$$

the size of the landing gear force f_i is computed from the footpad displacement and velocity (d_i & $\dot{d}_i$), and the spring damper coefficients (c_i & k_l) as shown below.

$$f_i = -k_l d_i - c_i \dot{d}_i \tag{48}$$

The spring constant k_l is constant and equal for all the landing gears, the damping coefficient c_i is the controllable variable. Three values are defined to be used in the computation of the damping coefficient, the nominal, minimum and maximum values of the damping coefficient.

$$c_{nom} \quad ; \quad c_{min} = 0.3 c_{nom} \quad ; \quad c_{max} = 3.0 c_{nom}$$

Taking into account that the lander has 4 legs and substituting from Eq. 48 the time derivative of the Lyapunov function can be written as,

$$\dot{V} = \sum_{i=1}^{4} \dot{V}_i = \sum_{i=1}^{4} -\alpha(k_l d_i + c_i \dot{d}_i)(\omega_x r_{iy} - \omega_y r_{ix})$$

$$= -\alpha \sum_{i=1}^{4} \left\{ \underbrace{c_i(\omega_x r_{iy} - \omega_y r_{ix})\dot{d}_i}_{term\ 1} + \underbrace{k_l(\omega_x r_{iy} - \omega_y r_{ix})d_i}_{term\ 2} \right\} \quad (49)$$

the optimum value of each damping coefficient c_i is chosen from c_{min} to c_{max} to minimize the time derivative of the Lyapunov function $\dot{V}$ by minimizing $\dot{V}_i$ for each landing gear. In Eq. 49, only term 1 can be manipulated by changing the value of the damping coefficient c_i, if the sign of $(\omega_x r_{iy} - \omega_y r_{ix})\dot{d}_i$ is positive then $\dot{V}_i$ is minimized by choosing a large damping coefficient and vice versa, on the other hand if the sign of $(\omega_x r_{iy} - \omega_y r_{ix})\dot{d}_i$ is negative then a small damping coefficient should be used. Consequently, the value for each damping coefficient c_i is calculated as,

$$c_i = \frac{c_{max} - c_{min}}{2}\{sgn[(\omega_x r_{iy} - \omega_y r_{ix})\dot{d}_i]\}\frac{c_{max} + c_{min}}{2} \quad (50)$$

4.3. Simulation and Results

The performance of the variable damper landing gear is evaluated for two common high-risk landing situations, landing with lateral velocity and landing on an inclined surface. For each situation the simulation is done with and without lateral propellant sloshing for a lander with a passive nominal landing gear and a lander with variable damper landing gear and the simulation results are analyzed and compared. Table 11 summarizes the simulation parameters.

Table 11: Variable damper landing gear simulation parameters

Parameter	Value	Unit
Dry body mass	600	kg
Sloshing propellant mass	100	kg
Initial vertical velocity	0.5	m/s
Slosh natural frequency	0.6	Hz
Tank radius	0.5	m
Surface spring constant	100	kN/m
Surface damping coefficient	0.1	kNs/m
Landing gear spring constant	1.0	kN/m
Landing gear nominal damping coefficient (c_{nom})	0.5	kNs/m

Landing gear variable damping coefficient	$0.3c_{nom} - 3.0c_{nom}$	kNs/m

4.3.1. Lateral Descent

Several simulations were conducted to examine the effectiveness of the variable damper landing gear in stabilizing a lander with a lateral velocity at touchdown in the presence of lateral propellant sloshing. Figure 30 shows the simulation results for a lander with passive landing gears without sloshing. Figure 30 (a) shows the simulation overview, figures 30 (b) and (c) show the attitude displacement and angular velocity of the lander, respectively. Figure 31 shows the simulation results for a lander with variable damper landing gears without sloshing. Figure 31 (a) shows the simulation overview, figures 31 (b) and (c) show the attitude displacement and angular velocity of the lander, respectively. Figure 32 shows the simulation results for a lander with variable damper landing gears with sloshing. Figure 32 (a) shows the simulation overview, figures 32 (b) and (c) show the attitude displacement and angular velocity of the lander, respectively. Table 12 summarizes the key parameter values of the simulation.

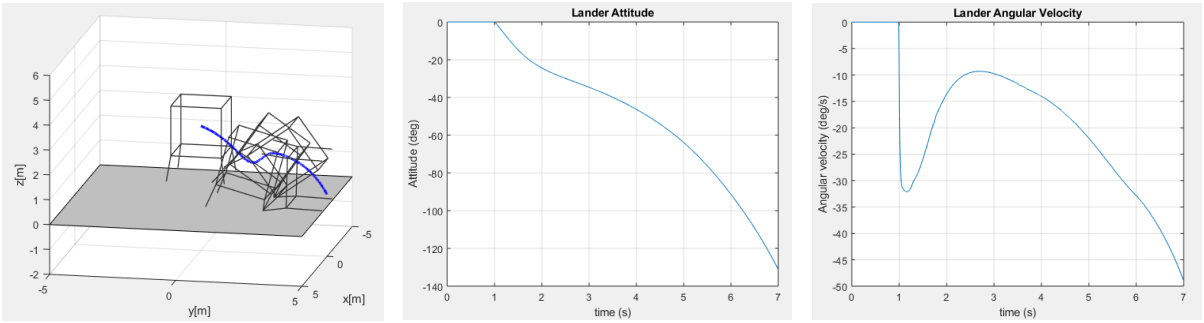

a) Overview b) Attitude displacement c) Angular velocity

Figure 30: Passive landing gear lateral descent simulation (w/o sloshing, gravity constant = 1.0 m/s^2, lateral velocity = 1.5 m/s)

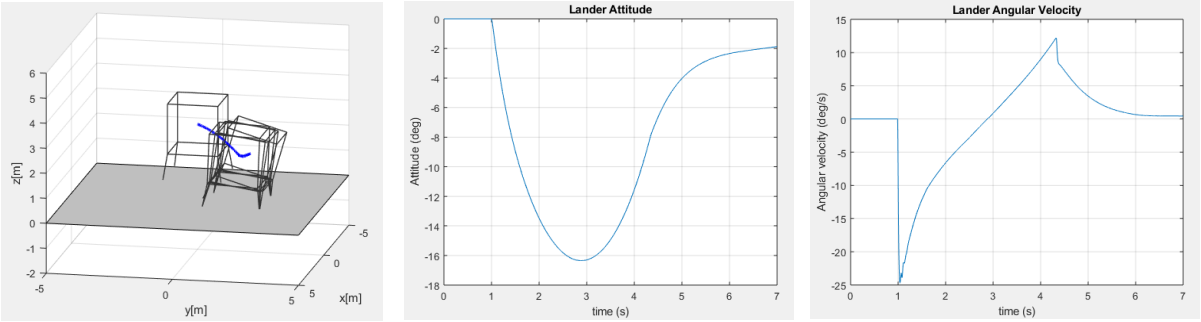

a) Overview b) Attitude displacement c) Angular velocity

Figure 31: Variable damper landing gear lateral descent simulation (w/o sloshing, gravity constant = 1.0 m/s^2, lateral velocity = 1.5 m/s)

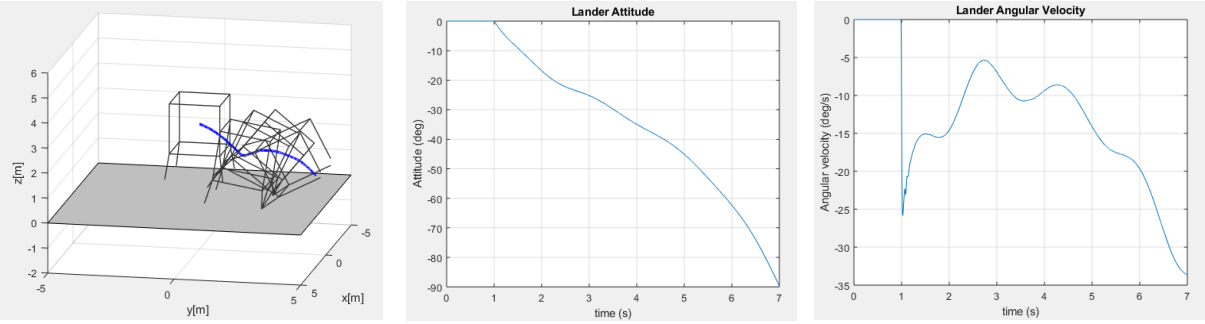

a) Overview b) Attitude displacement c) Angular velocity

Figure 32: Variable damper landing gear lateral descent simulation (w/ sloshing, gravity constant = 1.0 m/s^2, lateral velocity = 1.5 m/s)

The simulation results show that the variable damper landing gears equally enhances the stability of the lander with and without sloshing. However, it does not reduce the effect that lateral sloshing has on the lander stability as evident in table 10, the difference in the maximum stable velocity with and without sloshing is the same for both landing gear systems.

Table 12: Maximum stable lateral velocities w/ and w/o sloshing for landers with passive and variable landing gears (gravity constant = 1.0 m/s^2)

Landing gear	Maximum stable lateral velocity (m/s)		Difference (m/s)
	w/o Sloshing	w/ Sloshing	
Passive	1.29	1.02	0.27
Variable damper	1.66	1.40	0.26

4.3.2. Inclined Surface

Several simulations were conducted to examine the effectiveness of the variable damper landing gear in stabilizing a lander touchdown on an inclined surface in the presence of lateral propellant sloshing. Figure 33 shows the simulation results for a lander with passive landing gears without sloshing. Figure 33 (a) shows the simulation overview, figures 33 (b) and (c) show the attitude displacement and angular velocity of the lander, respectively. Figure 34 shows the simulation results for a lander with variable damper landing gears without sloshing. Figure 34 (a) shows the simulation overview, figures 34 (b) and (c) show the attitude displacement and angular velocity of the lander, respectively. Figure 35 shows the simulation results for a lander with variable damper landing gears with sloshing. Figure 35 (a) shows the simulation overview, figures 35 (b) and (c) show the attitude displacement and angular velocity of the lander, respectively. Table 13 summarizes the key parameter values of the simulation.

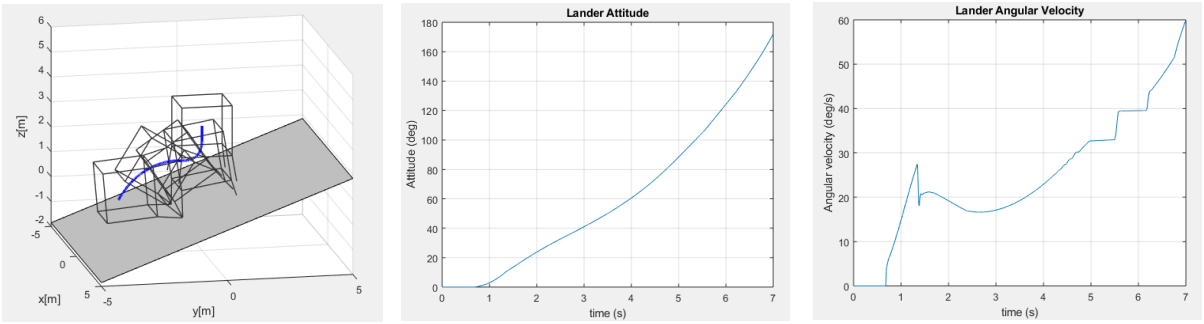

a) Overview b) Attitude displacement c) Angular velocity

Figure 33: Passive landing gear inclined surface simulation (w/o sloshing, gravity constant = 1.0 m/s2, inclination angle = 20 deg)

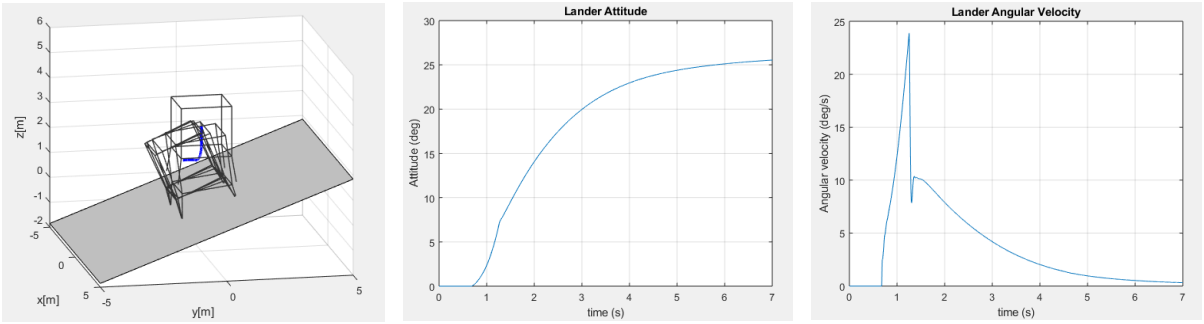

a) Overview b) Attitude displacement c) Angular velocity

Figure 34: Variable damper landing gear inclined surface simulation (w/o sloshing, gravity constant = 1.0 m/s2, inclination angle = 20 deg)

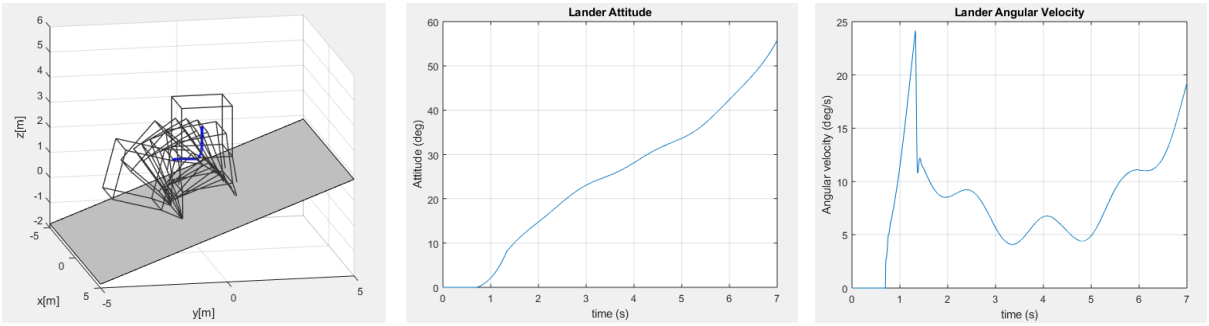

a) Overview b) Attitude displacement c) Angular velocity

Figure 35: Variable damper landing gear inclined surface simulation (w/ sloshing, gravity constant = 1.0 m/s2, inclination angle = 20 deg)

The simulation results show that the variable damper landing gears enhances the overall stability of the lander with and without sloshing. However, the effect of lateral sloshing on the lander stability is greater for a lander with variable damper landing gear as evident in table 11. The difference in the maximum stable inclination angle with and without sloshing is the notably higher in the case of a lander with variable damper landing gears.

Table 13: Maximum stable surface inclination w/ and w/o sloshing for landers with passive and variable landing gears (gravity constant = 1.0 m/s^2)

Landing gear	Maximum stable inclination (deg)		Difference (deg)
	w/o Sloshing	w/ Sloshing	
Passive	13.71	11.53	2.18
Variable damper	22.62	19.03	3.59

5. Conclusions and Future Work

5.1. Summary

This research investigates the effects of propellant sloshing in a partially filled tank on the dynamics and stability of landers. To do so, a simulation model of a lander is developed, the model consists of 3 main parts, the lander rigid body model, the landing gear model, and the propellant sloshing model. A mass-spring-damper model is used to characterize the behavior of liquid propellant in a partially filled spherical tank. The mathematical model of the lander system and its components is described in section 2. Section 3 presents the landing simulations and the obtained results. To provide a comprehensive and thorough analysis, the simulations are divided into 2 main parts, the first part investigates the effects of large amplitude propellant sloshing on a lander under low gravity conditions as in the case of asteroid or comet landers. The second part addresses the impact of lateral sloshing on a lander under high gravity conditions as in the case of planetary or lunar landers. In section 4, we evaluate the performance of variable damper landing gears proposed by Maeda et. al. [36] for planetary lander stabilization in the presence of lateral sloshing.

5.2. Obtained Results

For the case of low gravity simulations, the results suggest that large amplitude propellant sloshing in partially filled spherical tanks can have significant effects on the dynamics and behavior of the lander at touchdown. However, the nature of the sloshing effect and its extent are very dependent on external factors such as terrain conditions, lander velocity and direction, and tank position with respect to the lander center of mass. Though, in all the landing simulations, the results show that sloshing causes oscillatory behavior in the angular velocity of the lander which can be harmful as it can excite oscillations in other flexible components of the lander such as solar panels and appendages.

For the case of high gravity simulations, the stability of the lander is examined with and without lateral sloshing for 2 common high-risk situations, landing with lateral velocity and landing on an inclined surface, at several gravity constant values. The results reveal that for both situations, the presence of lateral sloshing deteriorates the stability of the lander at touchdown. Moreover, the results show that the effect of lateral sloshing becomes more apparent when increasing the value of the gravity constant.

For the variable damper landing gears, the performance of the system is examined in the same 2 high risk situations, landing with lateral velocity and landing on an inclined surface. In both situations, the variable damper landing gear improves the overall stability of the lander with and without sloshing. However, for the case of landing with lateral velocity, it does not reduce the effect that lateral sloshing has on the lander stability. Moreover, for the case of landing on an inclined surface, the effect of lateral sloshing on the lander stability is greater for a lander with variable damper landing gear

5.3. Future Work Recommendations

So far very few research studies have addressed the problem of propellant sloshing in landers. This thesis constitutes the first comprehensive study on the effects of propellant sloshing on planetary and small body landers, therefore there still exists several issues to be taken into consideration for future work. Several recommendations are presented below:

1- In all the simulations conducted in this thesis, the spacecraft is assumed to be unactuated and in ballistic descent, future studies may consider sloshing in actuated landers using thrusters.
2- Consider the presence of flexible components such as solar panels and appendages.
3- Design of active landing gears for planetary landers for suppressing lateral sloshing.
4- Use computational fluid dynamics (CFD) in the analysis instead of equivalent mechanical models to obtain more accurate results.

References

[1] Slabinski, V.J, Intelsat IV In-orbit Liquid Slosh Tests and Problems in the Theoretical Analysis of the Data, *Proc. Conf. Attitude Control of Space Vehicles: Technological and Dynamical Problems Associated with the Presence of Liquids*, Toulouse, France, ESA SP-129, 1977, pp. 87-102.

[2] O'Hern, E., Baddeley, V., and Rekowski, J., Analysis of Effects of Fluid Energy Dissipation on Spinning Satellite Control Dynamics, *AIAA Guidance and Control Conference*, AIAA 72-886, 1972.

[3] Strikwerda, T. E., Ray, J. C., Haley, D. R., and O'Shaughnessy, D. J., NEAR Shoemaker: Major Anomaly Survival, Delayed Rendezvous and Mission Success, *Proc. Conf. Attitude Control ofSpace Vehicles: Technological and Dynamical Problems Associated with the Presence of Liquids*, in Guidance and Control 2001, R.D. Culp and C.N. Schira, Eds. San Diego, CA: Univelt, 2001, pp. 597–614.

[4] Scholl, H. F., Pinson, L. D., and Stephens, D. G., Investigation of Slosh Anomaly in Apollo Lunar Module Propellant Gage, NASA-TM-X-2362, L-7757, 1971.

[5] Agrawal, B. N., Dynamic Characteristics of Liquid Motion in Partially Filled Tanks of a Spinning Spacecraft, *Journal of Guidance, Control, and Dynamics*, Vol. 16, No. 4, 1993, pp. 636–640.

[6] Nan, M., Junfeng, L., and Tianshu, W., Equivalent Mechanical Model of LargeAmplitude Liquid Sloshing Under Time-Dependent Lateral Excitations in Low-Gravity Conditions, *Journal of Sound and Vibration*, Vol. 386, 2017, pp. 421–432.

[7] Mason, P. and Starin, S. R., The Effects of Propellant Slosh Dynamics on the Solar Dynamics Observatory, *AIAA Guidance, Navigation, and Control Conference*, Portland, OR, Vol. 10, 2011, pp. 8768–8790.

[8] Sances, D., Gangadharan, S., Sudermann, J., and Marsell, B., CFD Fuel Slosh Modeling of Fluid-Structure Interaction in Spacecraft Propellant Tanks with Diaphragms, *51st, AIAA/ASME/ASME/ASCE/AHS/ASC Structures, Structural Dynamics and Materials Conference*, Orlando, FL, Vol. 8, 2010, pp. 6009-6017.

[9] Kos, L.D., Polsgrove, T.P., Sostaric, R.R, Braden, E.M., Sullivan, J.J., and Le, T.T. Altair Descent and Ascent Reference Trajectory Design and Initial Dispersion Analyses, *Proceedings of the AIAA Guidance, Navigation, and Control Conference, and Exhibit*, Toronto, Ontario, Canada, August 2010.

[10] Vreeburg, J.P.B, Spacecraft Maneuvers and Slosh Control, *IEEE Control Systems*, vol. 25, no. 3, pp. 12-16, June 2005.

[11] Sidi, M. J., Spacecraft Dynamics and Control, Cambridge Aerospace Series, Cambridge University Press, 1997.

[12] Dodge, F. T., The New Dynamic Behavior of Liquids in Moving Container, *Tech. Rep. NASA SP-106*, Southwest Research Institute, San Antonio, TX, 2000.

[13] Ibrahim, R. A., Liquid Sloshing Dynamics, Theory and Applications, Cambridge University Press, 2005.

[14] Man, G. K. and Eke, F. O., Effects of Payload Motions on the Nutational Stability of the Galileo Spacecraft, *Journal of Guidance, Control, and Dynamics*, Vol. 8, No. 6, 1985, pp. 683–688.

[15] Mingori, D. L. and Yam, Y., Nutational Instability of a Spinning Spacecraft with Internal Mass Motion and Axial Thrust, *AAS 86-2271, AIAA/AAS Astrodynamics Conference*, Williamsburg, VA, 1986, pp. 367–375.

[16] Or, A. C., Rotor-Pendulum Model for the Perigee Assist Module Nutation Anomaly, *Journal of Guidance, Control, and Dynamics*, Vol. 15, No. 2, 1992, pp. 297–303.

[17] Kane, T. R., Likins, P., and Levinson, D. A., Spacecraft Dynamics, Mc Graw-Hill, Inc., 1983.

[18] Kane, T. R. and Levinson, D. A., Dynamics Theory and Applications, Mc Graw-Hill, Inc., 1985.

[19] Banerjee, A. K., Contributions of Multibody Dynamics to Space Flight: A Brief Review, *Journal of Guidance, Control, and Dynamics*, Vol. 26, No. 3, 2003, pp. 385–394.

[20] Rackl, W., Lampariello, R., Parameter Identification of Free-Floating Robots with Flexible Appendages and Fuel Sloshing, *International Conference on Modelling, Identification & Control*, Dec. 2014.

[21] Roberts, J. R., Basurto, E. R., and Chen, P.-Y., Slosh Design Handbook l, *Northrop Space Lab, NASA Technical Report No. 27, Contract NAS 8-11111*, 1966.

[22] Kana, D. D., Validated Spherical Pendulum Model for Rotary Liquid Slosh, *Journal of Spacecraft and Rockets*, Vol. 26, 1989, pp. 188–195

[23] Nan, M., Junfeng, L., and Tianshu, B. Z., Large-Amplitude Sloshing Analysis and Equivalent Mechanical Modeling in Spherical Tanks of Spacecraft, *Journal of Spacecraft and Rockets*, Vol. 53, No. 3, 2016, pp. 500–506.

[24] Navabi, M. and Davoodi, A., 3D Multi-Pendulum Model of Slosh Dynamics in a Spacecraft, *Proceedings of 8th International Conference on Recent Advances in Space Technologies (RAST) IEEE*, 2017, pp. 259–262.

[25] Hervas, J. R. and Reyhanoglu, M., Thrust-Vector Control of a Three-Axis Stabilized Upper-Stage Rocket with Fuel Slosh Dynamics, *Acta Astronautica*, Vol. 98, 2014, pp. 120–127.

[26] Deng, M., Yue, B. and Yu, J., Position and Attitude Control of Spacecraft with Large Amplitude Propellant Slosh and Depletion, *Journal of Aerospace Engineering*, Vol. 30, Issue 6, 2017.

[27] Kubota, T., Sawai, S., Hashimoto, T., and Kawaguchi, J., Robotics and Autonomous Technology for Asteroid Sample Return Mission, *Proceedings of the 12th International Conference on Advanced Robotics*, 2005, pp. 31-38.

[28] Glassmeier, K.-H., Boehnhardt, H., Koschny, D., Kührt, E., Richter, I., The Rosetta Mission: Flying towards the origin of the solar system, *Space Science Reviews*, Vol. 128, Issue 1-4, 2007, pp. 1–21.

[29] Dunham, D.W., Farquhar, R., McAdams, J.V., Holdridge, M., Nelson, R., Whittenburg, K. Implementation of the First Asteroid Landing, *Icarus 159*, 2002, pp. 433–438.

[30] Kubota, T., Hashimoto, T., Sawai, S., Kawaguchi, J., Ninomiya, K., Uo, M., and Baba, K., An autonomous navigation and guidance system for MUSES-C asteroid landing, *Acta Astronautica*, Vol. 52, 2003, pp. 125–131.

[31] Tsuda, Y., Yoshikawa, M., Saiki, T., Nakazawa, S., and Watanabe, S., Hayabusa2– Sample return and kinetic impact mission to near-earth asteroid Ryugu, *Acta Astronautica*, Vol. 156, 2018, pp. 387-393.

[32] Ulamec, S., Biele, J., Blazquez, A., Cozzoni, B., Delmas, C., Fantinati, C., Gaudon, P., Geurts, K., Jurado, E., K¨uchemann, O., Lommatsch, V., Maibaum, M., Sierks, H., and Witte, L., Rosetta lander - Philae: landing preparations, *Acta Astronautica*, Vol.107, 2015, pp. 79–86.

[33] Bernard, J., Dufour, F., Gaudon, P., Ceolin, T., and Kerambrun, S., Rosetta mission analysis of the landing phase on a comet, *AIAA/AAS Astrodynamics Specialist Conference*, 2002.

[34] Witte, L., Roll, R., Biele, J., Ulamec, S. and Jurado, E., Rosetta lander Philae – Landing performance and touchdown safety assessment, *Acta Astronautica*, Vol. 125, 2016, pp. 149 – 160.

[35] Roll, R. and Witte, L., ROSETTA lander Philae: Touch-down reconstruction, *Planetary and Space Science*, Vol. 125, 2016, pp. 12–19.

[36] Maeda, T., Otsuki, M., Hishimoto, T., Attitude Stabilization for Lunar and Planetary Lander with Variable Damper, *Journal of Guidance, Control, and Dynamics*, Vol. 39, No. 8, 2016.

[37] Enright, P. and Wong, E., Propellant Slosh Models for the Cassini Spacecraft, *AIAA. Inc. with permission Jet Propulsion Laboratory*, California Institute of Technology, Pasadena, CA, 1994.

[38] Quadrelli, M., Modeling and Analysis for Nutation Time Constant Determination of On-Axis Diaphragm Tanks on Spinners: Application to the Deep Space One, *AAS/AIAA Space Flight Mechanics*, Ponce, Puerto Rico, 2003.

[39] Okhotsimskidi, E., Theory of the Motion of a Body with Cavities Partially Filled with a Liquid, NASA TT F-33, 1960.

[40] Rackl, W. Gerstmann, J. and Lampariello, R., Analysis of liquid fuel sloshing on free-floating robot dynamics under low-gravity condition, *IEEE Aerospace Conference*, Big Sky, MT, 2018.

[41] 小松敬治, スロッシング液面揺動とタクの振動, 森 北出版株式会社, 2015.